Numerical Computation of Spectra of Non-Hermitian Operators

Bachelors Thesis

presented by

Emma Falke

under the supervision of

Prof. Dr. Fabian Hassler

JARA-Institute for Quantum Information

February 2026

Abstract

This thesis investigates the existence of spectra of a class of non-Hermitian operators. We consider Hamiltonians of the form $H = p^2 + ipf(q) + g(q)$, which can be transformed into a standardized representation $H = p^2 + V(q)$ and analyzed under complex deformations. The numerical computation of spectra and eigenfunctions in a truncated Hermite basis can produce spurious eigenvalues and non-convergent eigenfunctions due to the basis cutoff. To distinguish physically meaningful eigenvalues from numerical artifacts, quantitative criteria for spectral validity are introduced. The numerical results are combined with an analysis of the asymptotic behavior of the wave functions. By examing the associated Stokes and anti-Stokes structure, we find that well-defined spectra exist away from the Stokes lines, while spectral definitions break down on the Stokes lines themselves.

Contents

Chapter 1

Introduction

In conventional quantum mechanics, quantum systems are typically described by Hermitian operators H which satisfy $H^\dagger = H$, where $H^\dagger$ denotes the adjoint of H. Hermitian operators have real eigenvalues and corresponding orthonormal eigenfunctions. This ensures unitary time evolution and the conservation of probability [1]. For closed quantum systems, this framework provides a consistent and well-established mathematical foundation.
However, many physically relevant systems cannot be described adequately using Hermitian operators alone. Non-Hermitian operators arise naturally in the effective description of open quantum systems. Unlike Hermitian operators, the eigenvalues of non-Hermitian operators can be complex and the eigenfunctions are no longer orthogonal [2]. Despite these differences, non-Hermitian quantum mechanics has been shown to admit physically meaningful and mathematically consistent structures. In particular certain classes of non-Hermitian systems, for example, $\mathcal{PT}$-symmetric Hamiltonians can have entirely real spectra and well-defined eigenfunctions [3]. Computing the eigenvalues and eigenfunctions of non-Hermitian operators can pose significant numerical challenges, [4,5] making it a central difficulty in studying such systems. Similar to the Hermitian case, one often expands the problem in a truncated basis of Hermite functions. These form a complete basis in $L^2(\mathbb{R})$ [6] and are well suited for polynomial Hamiltonians. For Hermitian operators, computations in this truncated basis are generally well behaved. However, in the non-Hermitian setting, this approach frequently leads to numerical instabilities, particularly for eigenvalues associated with higher basis indices. As a result, spurious eigenvalues or non-convergent eigenfunctions may appear [5].

This is why, in this thesis, we will focus on the computation and interpretation of spectra and eigenfunctions of various non-Hermitian operators within the Hilbert space of square-integrable functions. We aim to establish a method to test the existence of spectra. As a starting point, we consider the harmonic oscillator Hamiltonian as an example of a Hermitian quantum system. Building on this reference case, we introduce a complex deformation of the form $p \to p\exp(i\phi)$ and $q \to q\exp(-i\phi)$ to define a class of Hamiltonians. Within this framework we are going to compute the spectra of those Hamiltonians and

investigate how the existence of spectra depends on the asymptotic behavior of the eigenfunctions. To quantify this behavior, we introduce suitable quantities to discuss the spectral existence. In particular, we will introduce the system of Stokes and anti-Stokes lines, which governs the exponential growth or decay of solutions at infinity [7] and discuss the existence of spectra within the structure of those. Finally, we extend these insights to a broader class of non-Hermitian Hamiltonians of the form $H = p^2 + ipf(q) + g(q)$, where $f(q)$ and $g(q)$ are polynomial functions. We will show that by applying a transformation these can be brought into a standardized form, involving polynomial potentials. The results of the analysis of the complex deformed system are a powerful tool for determining the existence of spectra in this class. We therefore will cover several examples.

Chapter 2

Non-Hermitian Harmonic Oscillator

In this chapter we investigate the harmonic oscillator as a reference system for both analytical and numerical studies. We first review the exact solutions of the time-independent Schrödinger equation and introduce the harmonic oscillator eigenfunctions as a natural basis for functions in $L^2(\mathbb{R})$. Based on this, we discuss a numerical approach for computing eigenvalues and eigenfunctions using a truncated basis.
Then, we extend the analysis to a complex deformation of the harmonic oscillator Hamiltonian, which makes the system non-Hermitian, and examine how this modification affects the numerical spectrum and eigenfunctions.

2.1 Analytical Solutions of the Harmonic Oscillator

We start this chapter by discussing the time-dependent Schrödinger equation in one dimension. In real space it is given by

$$H\Psi(q,t) = \left[p^2 + V(q)\right]\Psi(q,t) = i\frac{\partial}{\partial t}\Psi(q,t), \tag{2.1}$$

where $H = p^2 + V(q)$ denotes the time-independent Hamiltonian of the system and $\Psi(q,t) \in \mathcal{H}$ is the wave function with $\mathcal{H} \in L^2(\mathbb{R})$. These operators satisfy the canonical commutation relation $[q,p] = i$. The operators p and q arise from a rescaling of the physical position and momentum operators [1]. This yields a one-dimensional Hamiltonian of the form $H = p^2 + V(q)$. For a time-independent potential $V(q)$, we can choose the separation ansatz

$$\Psi(q,t) = e^{-iEt}\psi(q). \tag{2.2}$$

Substituting into the time-dependent Schrödinger equation, see Eq. (2.1), yields

$$E\psi(q)e^{-iEt} = \left[-\psi''(q) + V(q)\psi(q)\right]e^{-iEt}. \tag{2.3}$$

Multiplying both sides by e^{iEt}, we obtain the time-independent Schrödinger equation

$$E\psi(q) = H\psi(q). \tag{2.4}$$

The original differential equation is thus reduced to an eigenvalue problem for the Hamiltonian operator. The wave functions $\psi(q)$ are eigenfunctions of the Hamiltonian H with corresponding eigenenergies E. For the dimensionless harmonic oscillator with Hamiltonian

$$H = p^2 + q^2 = -\frac{d^2}{dq^2} + q^2, \tag{2.5}$$

the time-independant Schrödinger equation, Eq. (2.4), yields the differential equation

$$-\psi''(q) + q^2\psi(q) = E\psi(q). \tag{2.6}$$

This is a second-order differential equation, so it has two linearly independent solutions. The general solution can be written as

$$\psi(q) = \phi^-(q) + \phi^+(q) = Af(q)e^{-q^2/2} + Bg(q)e^{q^2/2}. \tag{2.7}$$

with $A, B = const$. The wave-function belongs to the Hilbertspace $\mathcal{H} \in L^2(\mathbb{R})$ if it is square-integrable

$$\int_{-\infty}^{\infty} dq\, |\psi(q)|^2 < \infty, \tag{2.8}$$

where $|\psi(q)|^2 = \psi^*(q)\psi(q)$ and $\psi^*(q)$ denotes the complex conjugate of the wave function. For $|q| \to \infty$ the exponential part dominates both terms. Consequently, $\phi^+(q)$ is not square-integrable and does not belong to $L^2(\mathbb{R})$. To ensure a normalizable wave function, we therefore set $B = 0$. However, ϕ^+ will be relevant in the discussion of the non-Hermitian case, see Sec. 2.5. Substituting $\phi^-(q)$ into the Schrödinger equation (2.6) yields

$$f''(q) - 2qf'(q) + (E-1)f(q) = 0, \tag{2.9}$$

which can be solved using the Hermite polynomials, defined as

$$H_n(q) = e^{\frac{q^2}{2}} \left(q - \frac{d}{dq}\right)^n e^{\frac{q^2}{2}}. \tag{2.10}$$

The solution reduces to a Hermite polynomial with eigenenergies $E_n = 2n + 1$, where $n \in \mathbb{N}_0$. Therefore, the eigenfunctions can be written as

$$\psi(q) = Ae^{-q^2/2}H_n(q) =: \phi_n(q), \tag{2.11}$$

which satisfy the eigenvalue equation $H\phi_n(q) = E_n\phi_n(q)$. Normalizing $\phi_n(q)$ to unity yields the Hermite functions

$$\phi_n(q) = \frac{1}{\sqrt{2^n n!\sqrt{\pi}}} H_n(q)e^{-q^2/2}. \tag{2.12}$$

The Hermite functions form a complete orthonormal basis of the Hilbert space $L^2(\mathbb{R})$ with

$$\int_{-\infty}^{\infty} \phi_m^*(q)\phi_n(q) = \delta_{nm}. \tag{2.13}$$

This implies that any function $f(q) \in L^2(\mathbb{R})$ can be expressed as

$$f(q) = \sum_{n=0}^{\infty} c_n \phi_n(q), \tag{2.14}$$

with expansion coefficients

$$c_n = \int_{-\infty}^{\infty} dq\, \phi_n(q) f(q). \tag{2.15}$$

We have thus obtained the analytical solutions for the wave functions of the harmonic oscillator Hamiltonian, see Eq. (2.5).

2.2 Numerical Implementation in the Hermite Basis

For the numerical computation we choose the basis of the Hermite functions. Therefore, we first discuss the expansion of eigenfunctions a little bit more precise. As an illustrative example, we consider the function $f(q) = e^{\alpha q^2}$ with $\alpha \in \mathbb{R}$ and seek to expand this function in the Hermite basis. The expansion coefficients c_n can be calculated as

$$c_n = \int_{-\infty}^{\infty} dq\, \phi_n(q) f(q) = \frac{\pi^{-1/4}}{\sqrt{2^n n!}} \int_{-\infty}^{\infty} dq\, e^{-(\frac{1}{2}-\alpha)q^2} H_n(q). \tag{2.16}$$

The Hermite functions $\phi_{2n}(q)$ are even, whereas $\phi_{2n+1}(q)$ are odd. Since $f(q)$ is even in this example, it follows immediatly that $c_{2n+1} = 0$ for all $n \in \mathbb{N}$. The even Hermite polynoms can be written in the form of [1]

$$H_{2n}(q) = \sum_{s=0}^{n} (-1)^s (2q)^{2(n-s)} \frac{(2n)!}{(2n-2s)!s!}. \tag{2.17}$$

Substituting into (2.16) yields

$$c_{2n} = \frac{2^{2(n-s)}\pi^{-1/4}}{\sqrt{2^{2n}(2n)!}} \sum_{s=0}^{n} \frac{(-1)^s (2n)!}{(2n-2s)!s!} \int_{-\infty}^{\infty} dq\, q^{2(n-s)} e^{-(\frac{1}{2}-\alpha)q^2}. \tag{2.18}$$

The integral appearing here is a Gaussian integral which converges for $\alpha < \frac{1}{2}$ and evaluates to

$$\int_{-\infty}^{\infty} dq\, q^{2(n-s)} e^{-(\frac{1}{2}-\alpha)q^2} = \frac{1}{\left[2(\frac{1}{2}-\alpha)\right]^{n-s}} \sqrt{\frac{\pi}{\frac{1}{2}-\alpha}} \frac{[2(n-s)]!}{2^{n-s}(n-s)!}. \tag{2.19}$$

Substituting this result into (2.18) and simplifying by using the binomial identity

$$(a+b)^n = \sum_{s=0}^{n} \binom{n}{s} a^k b^{n-s}, \tag{2.20}$$

[1] [8, see Eq. (13.9)]

then yields

$$c_{2n} = \frac{\pi^{1/4}}{2^n n!}\sqrt{\frac{(2n)!}{\frac{1}{2}-\alpha}}\left(\frac{\frac{1}{2}+\alpha}{\frac{1}{2}-\alpha}\right)^n. \tag{2.21}$$

Using Stirling's approximation, $n! \propto \sqrt{2\pi n} n^n e^{-n}$, it can be shown that

$$c_{2n} \propto \left(\frac{\frac{1}{2}+\alpha}{\frac{1}{2}-\alpha}\right)^n n^{-1/4} \tag{2.22}$$

for large n. Consequently, the expansion coefficients converge only if $\alpha < 0$ which is equivalent to $\exp(\alpha q^2)$ being square-integrable. But formal expansion of the Hermite coefficients is possible for $\alpha < 1/2$.

The distinction between formal expansions and convergence in $L^2(\mathbb{R})$ becomes relevant for non-Hermitian Hamiltonians, which arise in the complex-deformed systems studied in the next section. For a non-Hermitian operator $H \neq H^\dagger$, one must distinguish between right and left eigenfunctions $\psi_R(q)$ and $\psi_L(q)$, defined by

$$H\psi_R(q) = E\psi_R(q), \qquad H^T\psi_L(q) = E^*\psi_L(q), \tag{2.23}$$

where E^* denotes the complex conjugated of E. This includes that the eigenvalues E do not necessarily have to be real. Square-integrability is expressed through

$$\int_{-\infty}^{\infty} dq\, \psi_L^*(q)\psi_R(q) < \infty. \tag{2.24}$$

In this setting, it is not required that the individual expansions of the left and right eigenfunctions converge term by term, as long as their product is integrable

$$\int_{-\infty}^{\infty} dq\, \psi_L^*(q)\psi_R(q) = \int_{-\infty}^{\infty} dq\, \left(\sum_{n=0}^{\infty} c_n\phi_n(q)\right)^* \left(\sum_{n=0}^{\infty} d_m\phi_m(q)\right) < \infty. \tag{2.25}$$

We will revisit the definition of left and right eigenfunctions in subsequent sections of this thesis (see Sec. 2.4). However, these observations show that in terms of $f(q) = \exp(\alpha q^2)$ a formal representation in the Hermite basis is possible for $\alpha < \frac{1}{2}$, even though the series converges in $L^2(\mathbb{R})$ only if $\alpha < 0$. For the left and right eigenfunctions, it is sufficient that the product $\psi_L^*(q)\psi_R(q)$ is integrable. However, as long as the overall inner product remains integrable, the individual expansions may converge more slowly.

We now turn to the numerical computation of eigenvalues and eigenfunctions of the harmonic oscillator. To this end, we formulate the problem in the basis of the Hermite functions, introduced in Sec. 2.1. We introduce the ladder operators

$$a = \frac{1}{\sqrt{2}}(q + ip), \qquad a^\dagger = \frac{1}{\sqrt{2}}(q - ip), \tag{2.26}$$

which satisfy the commutation relation $\left[a, a^\dagger\right] = 1$. Consequently, the harmonic oscillator Hamiltonian, from Eq. (2.5), can be written as

$$H = 2a^\dagger a + 1 = 2N + 1, \tag{2.27}$$

where $N = a^\dagger a$ denotes the number operator. Its eigenstates $|n\rangle$, also called Fock states, are defined by

$$N|n\rangle = n|n\rangle, \qquad n = 0, 1, 2, \ldots \tag{2.28}$$

and are simultaneously eigenstates of H. The ladder operators act on the Fock states as

$$a|n\rangle = \sqrt{n}|n-1\rangle, \qquad a^\dagger|n\rangle = \sqrt{n+1}|n+1\rangle. \tag{2.29}$$

All eigenstates can therefore be generated from the ground state $|0\rangle$, defined by $a|0\rangle = 0$, via

$$|n\rangle = \frac{(a^\dagger)^n}{\sqrt{n!}}|0\rangle. \tag{2.30}$$

In position space, the corresponding eigenfunctions $\phi_n(q) = \langle q \mid n\rangle$ are obtained by solving

$$a\phi_0(q) = \frac{1}{\sqrt{2}}\left(q + \frac{d}{dq}\right)\phi_0(q) = 0. \tag{2.31}$$

This yields the well-known Hermite functions

$$\phi_n(q) = \frac{1}{\sqrt{2^n n!\sqrt{\pi}}} H_n(q)\, e^{-q^2/2}, \tag{2.32}$$

with eigenvalues $E_n = 2n + 1$.

We now aim to compute the eigenvalues and eigenfunctions of the harmonic oscillator numerically. To do this, we formulate the problem in the Hermite basis, which is an infinite-dimensional basis of $L^2(\mathbb{R})$. Since it is not possible to compute an infinite number of eigenvalues and eigenvectors, we approximate the problem using a truncated basis of Hermite functions of dimension N. In this basis the ladder operators are represented as $N \times N$ matrices with elements determined by their action on the Fock states. This means that

$$a = \begin{pmatrix} 0 & \sqrt{1} & 0 & \cdots & \cdots & 0 \\ 0 & 0 & \sqrt{2} & 0 & \cdots & 0 \\ \vdots & \vdots & \ddots & \ddots & \ddots & \vdots \\ \vdots & \vdots & \ddots & \ddots & \sqrt{N-2} & 0 \\ \vdots & 0 & \cdots & \cdots & 0 & \sqrt{N-1} \\ 0 & \cdots & \ldots & \cdots & \cdots & 0 \end{pmatrix} \tag{2.33}$$

and $a^\dagger = a^T$. The position and momentum operators are then given by

$$q = \frac{1}{\sqrt{2}}(a^\dagger + a), \qquad p = \frac{i}{\sqrt{2}}(a^\dagger - a). \tag{2.34}$$

Substituting these expressions into the Hamiltonian yields its matrix representation in the truncated Hermite basis. The eigenvalues and corresponding eigenvectors of this matrix can then be computed numerically. The eigenvalues are sorted in order of increasing absolute value. For a truncated basis of dimension N, this procedure yields N eigenvalues E_n and corresponding eigenvectors v_n, with $n = 0, 1, \ldots, N-1$. Each eigenvector v_n consists of N components

$$v_n = \left.\begin{pmatrix} c_0^{(n)} \\ c_1^{(n)} \\ \vdots \\ c_{N-1}^{(n)} \end{pmatrix}\right\} N, \tag{2.35}$$

which define the expansion of the nth eigenfunction in the truncated Hermite basis. In the real space, the corresponding approximate eigenfunction is given by

$$\psi_n(q) = \sum_{i=0}^{N-1} c_i^{(n)} \phi_i(q). \tag{2.36}$$

In the following, we will refer to N as the basis size or cutoff of the basis. This representation implies that the eigenfunctions can only be computed up to the chosen cutoff N. For the harmonic oscillator, the nth eigenfunction is exactly given by the nth Hermite function. Accordingly, the numerical eigenvector v_n is expected to have a single nonvanishing component at index n. In general, the computation of eigenvalues and eigenfunctions, in the truncated Hermite basis, can be performed for Hermitian and non-Hermitian operators.

2.3 Complex Deformation of the Harmonic Oscillator

In the previous section, we developed a numerical framework for computing eigenvalues and eigenfunctions of operators in the truncated Hermite basis. Building on this framework, we now extend the analysis to include a complex deformation of the harmonic oscillator Hamiltonian from Eq. (2.5). Specifically, we investigate its behavior under a rotation in the complex plane. The transformation is defined by

$$p \to e^{i\phi} p, \qquad q \to e^{-i\phi} q, \tag{2.37}$$

with $\phi \in [0, 2\pi)$. The commutator relation is preserved with

$$\left[e^{-i\phi} q, e^{i\phi} p\right] = e^{-i\phi} q e^{i\phi} p - e^{i\phi} p e^{-i\phi} q = [q, p] = i. \tag{2.38}$$

The Hamiltonian becomes

$$\tilde{H} = p^2 e^{2i\phi} + q^2 e^{-2i\phi}, \tag{2.39}$$

which is in general no longer Hermitian.

The computation of eigenvalues and eigenvectors can be performed as described in the previous section. The computed eigenvalues are shown in Figure 2.1 for $\phi \in [0, 2\pi)$. Several energy eigenvalues are plotted as functions of ϕ, for a cutoff $N = 200$. As described in Sec. 2.2, the eigenvalues are ordered according to increasing absolute value. Therefore E_0 denotes the eigenvalue with the smallest

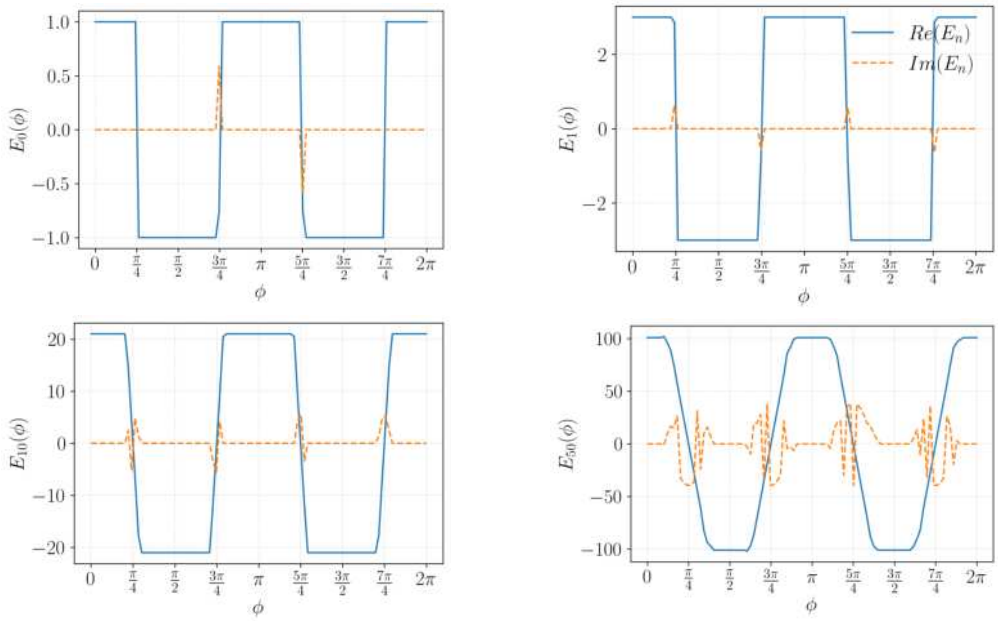

Figure 2.1: E_0, E_1, E_{10} and E_{50} plotted as functions of the angle ϕ for $N = 200$. For $\phi = \frac{(2k+1)\pi}{4}$ a sharp transition between the positive and the negative eigenvalue of $E_n = 2n+1$ is observable. With increasing index of the eigenstates this transition becomes increasingly less steep.

absolute value in the spectrum. Figure 2.1 shows an oscillatory dependence of the eigenvalues on the deformation angle ϕ. For $\phi = 0$ the eigenenergies take the expected harmonic-oscillator values $E_n = 2n + 1$ and remain constant with increasing ϕ. At $\phi = \frac{\pi}{4}$ however, the low eigenvalues undergo a sharp transition to negative values. Additional discontinuous changes occur at $\phi = \frac{(2k+1)\pi}{4}$ with $k = 0, 1, 2, 3$. While similar behavior is observed for higher eigenvalues, the corresponding transitions become increasingly less steep and appear to "smear out". This is a consequence of the truncated Hermite basis.

To gain a better understanding of this we discuss the Hamiltonian of Eq. (2.39) with $\phi = \frac{\pi}{8}$, which remains in the area where E_n is positive. The resulting computed energy spectrum, of this particular angle, for three cutoff values N, is shown in Fig. 2.2. We observe that the lowest eigenvalues remain on the real axis and appear at similar positions for all three cutoffs. In contrast, higher eigenvalues exhibit significant shifts in their imaginary parts. Higher-index

eigenvalues deviate from the real axis. In this context, for smaller cutoff values, such as, $N = 10$ the number of eigenvalues E_n on the real axis is significantly smaller than for larger cutoff values such as $N = 100$.

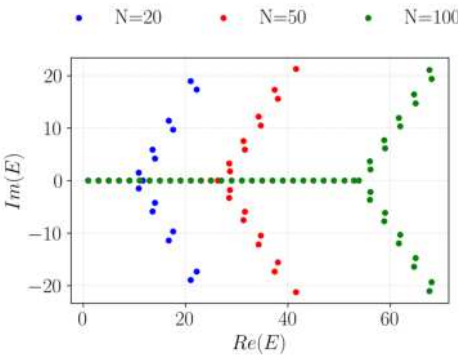

Figure 2.2: Energy spectrum of the rotated harmonic oscillator for $\phi = \frac{\pi}{8}$ for several N. Shown are all E_n for $N = 20$, the first 32 eigenvalues for $N = 50$, and the first 48 eigenvalues for $N = 100$.

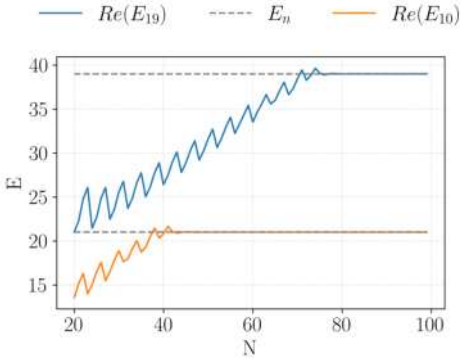

Figure 2.3: Real parts of the eigenvalues E_{10} and E_{19} as functions of the Hamiltonian's basis size N, showing clear convergence to the corresponding eigenvalues E_n of the untransformed Hamiltonian.

Exemplarly, Fig.2.3 displays the real parts of two eigenvalues as functions of the Hamiltonian's basis size N. As N increases, the eigenvalues converge to the corresponding eigenvalues $E_n = 2n + 1$ of the untransformed Hamiltonian. From these observations, we conclude, that the basis size affects the number of eigenvalues that converge.

Figure 2.4 shows the distributions of the components c_i of the right eigenvectors v_n for $N = 100$, plotted as a function of the basis index i. For low eigenstates, the eigenvector components are concentrated near small basis indices and decay rapidly toward higher indices. In contrast, eigenvectors associated with higher-index eigenvalues are increasingly dominated by components at large basis indices. The components remain significant or even increase near the cutoff.

These behaviors reflect numerical effects that arise when computing the spectrum and eigenfunctions of non-Hermitian Hamiltonians, using a truncated Hermite basis. In such systems, the computed eigenstates may become strongly localized near the highest-index basis states. Due to the truncation of the basis high-indexed eigenvalues and eigenvectors deviate from the actual eigenvalues and eigenvectors of the spectrum. Therefore, they become spurious and cannot be reliably identified as part of the spectrum. In contrast, eigenvalues and eigenvectors that are localized within the low-index portion of the basis remain largely unaffected by the basis size. Increasing the cutoff N enlarges the number of stabilized eigenvalues and eigenvectors, as illustrated in Fig. 2.2.
Motivated by these effects, we address the question of how to quantify whether

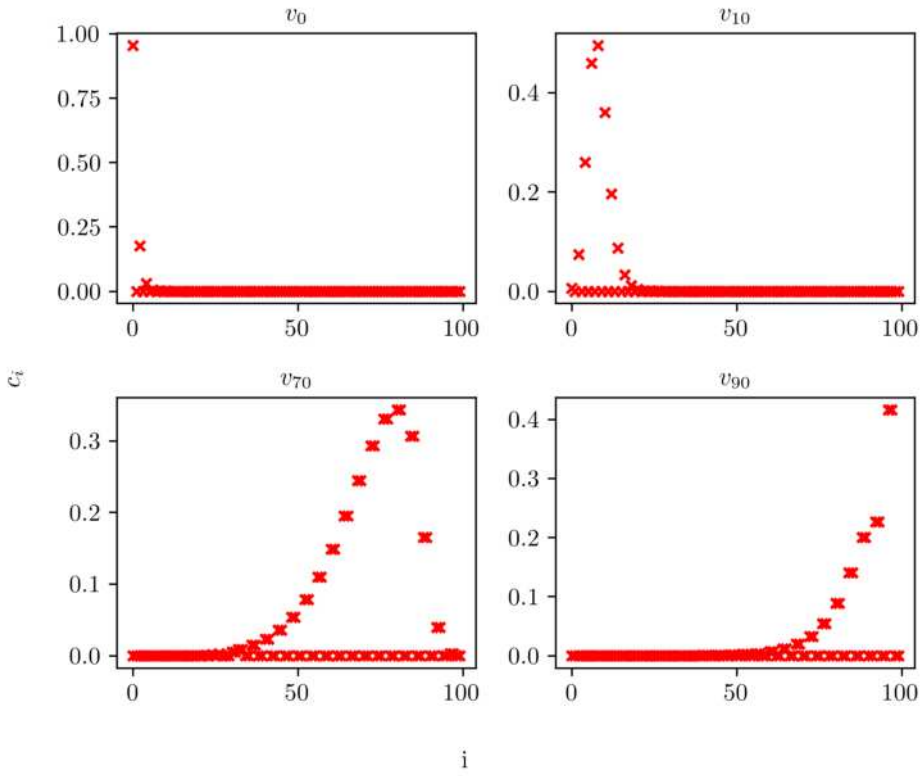

Figure 2.4: Structure of the eigenvectors of the rotated harmonic oscillator for $\phi = \frac{\pi}{8}$ and $N = 100$. Higher-index eigenvectors retain significant components near the cutoff.

an eigenvalue and its corresponding eigenvector can be reliably considered part of the spectrum. In the following section, we introduce two quantities that allow us to discuss the stability and authenticity of the computed spectra.

2.4 Verification of Spectral Existence

We aim to make a quantitative statement about which eigenvalues of the non-Hermitian Hamiltonian of Eq.(2.39) can be considered part of the spectrum. To this end, we define two quantities that characterize the stability and convergence of the corresponding eigenvectors.
As a reminder, for a non-Hermitian Hamiltonian, the right and left eigenvectors can differ, and the standard orthonormality of Hermitian systems no longer holds. The right and left eigenvectors $|w_n\rangle$ and $|\tilde{w}_n\rangle$ satisfy

$$H|w_n\rangle = E_n|w_n\rangle, \qquad \langle\tilde{w}_n|H = \langle\tilde{w}_n|E \Leftrightarrow H^T|\tilde{w}_n\rangle = E^*|\tilde{w}_n\rangle. \tag{2.40}$$

When represented in real space, the right and left eigenstates are reduced to the right and left eigenfunctions $\psi_{R,n}(q)$ and $\psi_{L,n}(q)$, introduced in Eq. (2.23). One numerical effect, arising from the truncation of the Hermite basis, is the accumulation of eigenvector weight in the high-index part of the basis, as shown

in Fig. 2.4. For eigenvalues that do not depend on the basis size and therefore belong to the stable part of the spectrum, the eigenvector components are mostly localized in the low-index region.
To quantify this behavior and evaluate the stability of the corresponding eigenvalue E_n, we compare the weight contained in the lower- and higher-index parts of the eigenvector. Therefore we define the quantity y by

$$y_n = \frac{\sum_{i=N}^{2N} |d_i \tilde{d}_i|}{\sum_{i=0}^{N} |d_i \tilde{d}_i|}, \tag{2.41}$$

where d_i and $\tilde{d}_i$ denote the components of the right eigenvector w_n and the left eigenvector $\tilde{w}_n$ respectively. The total vector length is $2N$. The quantity y_n compares the weight of the nth eigenvector contained in the first N basis components with the weight contained in the second half of the vector. A small y_n indicates that the eigenvector is concentrated in the low-index portion of the basis. Conversely, large y_n signals accumulation near the cutoff are indicating a numerically unstable eigenvalue. For this reason, y_n is referred to as the tail-weight ratio. Consequently, if E_n is part of the spectrum, y_n is expected to decrease and approach zero as the cutoff N is increased.

Figure 2.5 shows the tail-weight ratio y plotted as a function of the cutoff N, for $\phi = \frac{\pi}{8}$. Exemplary, the first three and the ninth eigenstate are shown here. We observe that with increasing N, y_n increases towards a signifiant small numerical value. Therefore we can conclude that for $\phi = \frac{\pi}{8}$ the eigenvectors remain predominantly localized in the low-index region of the basis.

Next, we want to compare how the right and left eigenvectors of the non-Hermitian Hamiltonian change, when the size of the basis is doubled. Therefore, we calculate two sets of left and right eigenvectors. The right and left eigenvectors corresponding to the eigenvalue E_n in a basis of length $2N$ are again denoted by w_n and $\tilde{w}_n$ with components d_i and $\tilde{d}_i$, respectively, while v_n and $\tilde{v}_n$ with components c_i and $\tilde{c}_i$ denote the corresponding eigenvectors obtained in a basis of length N.
For that to remain unaffected by the truncation of the basis, we expect the first N components of the eigenvectors w_n and v_n to coincide, while the additional N components of w_n should be small. To quantify this similarity, we use the Cauchy–Schwarz inequality, which for two complex vectors x and y is defined to be

$$|\sum_{k=0}^{N} x_k y_k^*|^2 \leq \sum_{k=0}^{N} |x_k|^2 \sum_{k=0}^{N} |y_k|^2, \tag{2.42}$$

where y^* denotes the complex conjugated of y. Equality holds if and only if these two vectors are linearly dependent. We define $x_k = d_i \tilde{d}_i$ and $y_k = c_i \tilde{c}_i$ and the quantity z_n is introduced as

$$z_n = \frac{|\sum_{i=0}^{N} d_i \tilde{d}_i (c_i \tilde{c}_i)^*|^2}{\sum_{i=0}^{N} |d_i \tilde{d}_i|^2 \sum_{i=0}^{N} |c_i \tilde{c}_i|^2}. \tag{2.43}$$

The quantity z_n should increase with increasing cutoff N and approach unity in the limit of convergence. In conclusion, z_n is a measure for the similarity of eigenvectors obtained with different basis sizes. In the following, z_n will be referred to as the truncation fidelity.

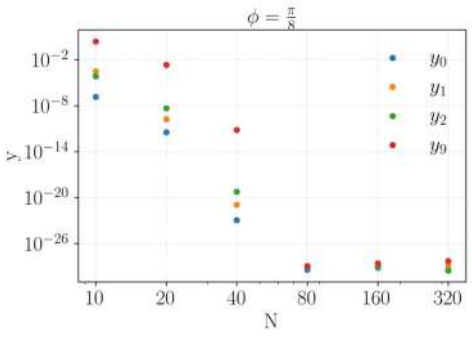

Figure 2.5: Tail-weight-ratio y_n as a function of the cutoff N, for the complex deformed harmonic oscillator Hamiltonian with $\phi = \frac{\pi}{8}$. The first ten eigenvectors show significant convergence.

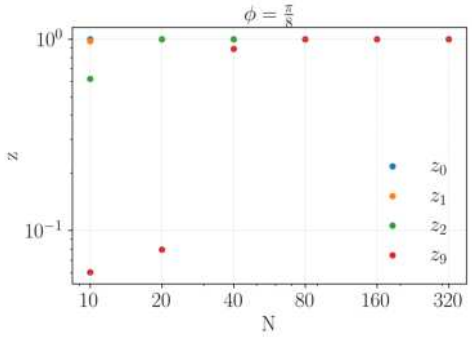

Figure 2.6: Truncation fidelity z_n as a function of the cutoff N, for the complex deformed harmonic oscillator Hamiltonian with $\phi = \frac{\pi}{8}$. z_n shows siginificant convergence to unity for the first ten eigenstates.

Figure 2.6, illustrates the truncation fidelity z_n as a function of the basis cutoff N, for $\phi = \frac{\pi}{8}$. We observe that z_n converges to unity for the first ten eigenstates. As discussed this indicates that these eigenvectors are insensitive to the basis size once $N \geq 80$. Consequently, the corresponding eigenvalues can be considered as part of the spectrum.
The quantities y_n and z_n establish a practical criterion for testing the stability and convergence of eigenstates of non-Hermitian Hamiltonians. Eigenstates that satisfy both of these criteria are unaffected by effects arising from the truncated Hermite basis. Therefore they can be identified as belonging to the stable part of the spectrum. Moreover, as the cutoff is increased an increasing number of eigenstates exhibits convergence of y_n and z_n. With increasing N more and more eigenstates will converge. In particular, for $\phi = \frac{\pi}{8}$, this indicates that the computation of eigenfunctions and eigenvalues in the Hermite basis yields a well-defined and physical spectrum.

In Fig. 2.1 we have seen that sharp transitions appear at the deformation angles $\phi = \frac{(2k+1)\pi}{4}$ with $k = 0, 1, 2, 3$. Examplarly for those angles, we investigate the behavior of y_n and z_n for the angle $\phi = \frac{\pi}{4}$. This behavior is shown in Fig. 2.7 and Fig. 2.8. The values of y_n appear to converge. This indicates that for $\phi = \frac{\pi}{4}$ the eigenvectors remain predominantly localized in the low-index region of the basis. However for the truncation fidelity in Fig. 2.8 it is observed that z_n converges to a value of order 10^{-1}. In this case, the eigenvectors w_n and v_n, respectively, do not appear to coincide in their components, regardeless the basis size. From the previous statements, we can therefore conclude that in the case of $\phi = \frac{\pi}{4}$ there are no converging eigenvectors and thus no physically

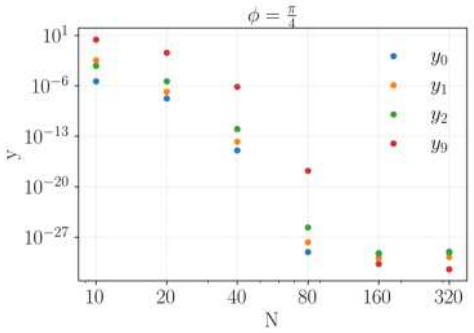

Figure 2.7: Tail-weight-ratio as a function of the cutoff N for $\phi = \frac{\pi}{4}$. The eigenvectors exhibit significant convergence.

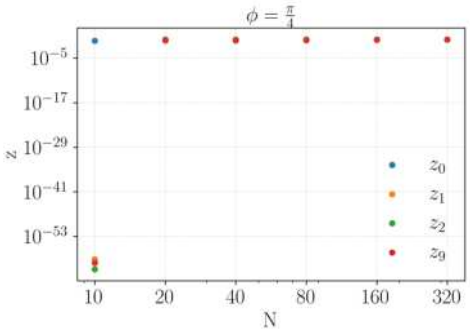

Figure 2.8: Truncation fidelity as a function of the cutoff N for $\phi = \frac{\pi}{4}$. No convergence towards zero is observed and therefore no spectrum exists.

stable spectrum exists.

The test of tail-weight-ratio and truncation fidelity can be performed for several angles in the unit circle. The result is always the same. Correct converging values can be found everywhere except for the angles of $\phi = \frac{(2k+1)\pi}{4}$[2].
The numerically computed energy spectra for $N = 200$, for several values of ϕ in the first quadrant of the unit circle, are shown in Fig. 2.9. For $\phi \in \left[0, \frac{\pi}{4}\right)$ the real part of E is positive while for $\phi \in \left(\frac{\pi}{4}, \frac{\pi}{2}\right]$ $Re(E_n) < 0$. At $\phi = 0$ and $\phi = \frac{\pi}{2}$ the Hamiltonian reduces to $H = \pm(p^2 + q^2)$ and all N eigenvalues lie on the real axis. Examining the number of stable eigenvalues on the real axis, we observe that as ϕ approaches $\frac{\pi}{4}$, this number gradually decreases. At $\frac{\pi}{4}$ itself, it appears that no significant number of eigenvalues have $Re(E_n) = 0$. This is consistent with the observation and discussion of tail-weight-ratio and truncation fidelity. For $\phi = \frac{\pi}{4}$ all eigenvalues and eigenvectors are strongly affected by the truncation of the basis. The computation of spectra yields no physically meaningful eigenvalues. Therefore no spectrum exists.

We have thus discussed the verification of spectra from a numerical perspective. In the next section, we will investigate the wave functions of the complex deformed Hamiltonian in Eq. (2.39) and study the existence of decaying or oscillatory solutions of the wave functions.

2.5 Asymptotic Behavior and Stokes Sectors

In Fig. 2.1, in Sec. 2.2, we have observed that the angles $(2k + 1)\pi/4$, with $k = 0, 1, 2, 3$, exhibit sharp transitions between the positive and negative value of E_n. In this section, we aim to analyze this behavior in more detail. In particular, we will focus on how the complex deformation of the harmonic oscillator modifies the asymptotic behavior of the eigenfunctions. Depending on

[2]Examples for this are attached in the Appendix (see Fig. 1, 2, 3, 4,5,6)

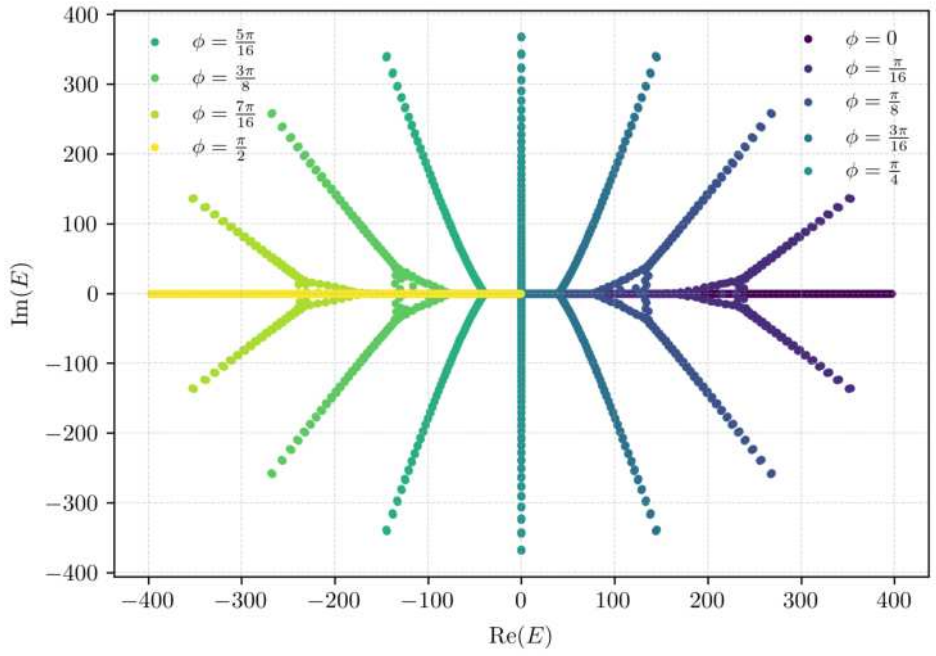

Figure 2.9: Numerically computed energy spectra for $N = 200$ at various angles, in the first quadrant of the unit circle.

the deformation angle ϕ, solutions may be oscillatory or exponentially decaying, which directly affects their normalizability and the convergence of their expansion in the Hermite basis.

As shown in Sec. 2.1, the general solution of the untransformed harmonic oscillator consists of two linearly independent solutions, see Eq. (2.7). For the wave function to be normalizable, its asymptotic behavior is crucial. For large q, the solutions are dominated by their exponential terms, and therefore the terms of the wave function satisfy

$$\phi_+(q) \propto \exp\left(+\frac{q^2}{2}\right), \quad \phi_-(q) \propto \exp\left(-\frac{q^2}{2}\right). \tag{2.44}$$

The sign in the exponent is determined by the requirement of normalizability. Applying the complex deformation $q \to qe^{-i\phi}$, $p \to pe^{i\phi}$ from Eq. (2.37) transforms the wave function $\psi(q) =\propto \phi_\pm(q)$ to

$$\psi(q) \propto \exp\left(\pm\frac{q^2}{2}e^{-2i\phi}\right) = \underbrace{\exp\left(\pm\frac{q^2}{2}\cos(2\phi)\right)}_{\in\mathbb{R}} \underbrace{\exp\left(\mp i\frac{q^2}{2}\sin(2\phi)\right)}_{\in\mathbb{C}}. \tag{2.45}$$

The first factor of the wave function is purely real, while the second factor is complex and oscillatory. In general, a decaying solution exists if and only if $\psi(q)$ decays for $q \to \infty$, so that the wave function is normalizable. This condition is controlled by the real part of the exponent. In case of the transformed wave

function, converging solutions occur when $\pm\cos(2\phi) < 0$. Then the real part of the exponent is negative. For $\cos(2\phi) < 0$ or $\cos(2\phi) > 0$, one can always find the appropiate sign in the exponent to ensure that $|\psi(q)|$ decays at infinity. The coefficient of the other linearly independent solution is then set to zero to ensure normalizable behavior. For $\sin(2\phi) = 0$ the complex part of the exponent is zero. No oscillatory part of the wave function exists.
For $\cos(2\phi) = 0$ the first factor the wave function becomes pruely oscillatory, thus no decaying solution and exists. Figure 2.11 illustrates the regions on

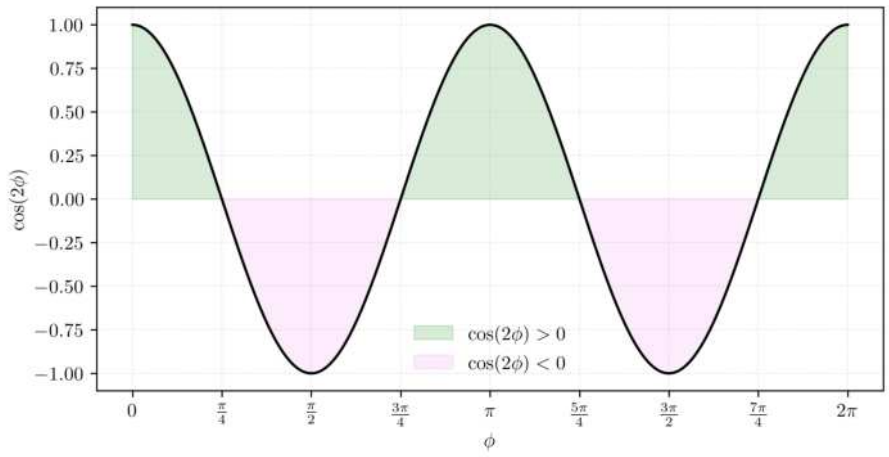

Figure 2.10: $\cos(2\phi)$ plotted as a function of ϕ. The green regions show parts where $\cos(2\phi) > 0$ and in the pink regions $\cos(2\phi) < 0$.

the unit circle in which decaying solutions of the wave function exist. In the pink regions, the decaying part of the wave function takes the form $\psi(q) \propto \exp(-\cos(2\phi)q^2/2)$ which requires $\cos(2\phi) < 0$ as shown in Fig. 2.10. The green regions correspond to solutions of the form $\psi(q) \propto \exp(+\cos(2\phi)q^2/2)$ for which $\cos(2\phi) > 0$. The boundaries between these regions are given by $\cos(2\phi) = 0$, where no decaying solutions of the wave function exist. For the harmonic oscillator they are located at

$$\phi_{st} = \left[\frac{\pi}{4}, \frac{3\pi}{4}, \frac{5\pi}{4}, \frac{7\pi}{4}\right], \tag{2.46}$$

and will be referred to as Stokes lines in the following sections. In contrast, the directions for which the wave function is purely exponential (i.e., the oscillatory part vanishes) and a "perfectly" decaying solution exists are called anti-Stokes lines. For the harmonic oscillator they are located at

$$\phi_{ast} = \left[0, \frac{\pi}{2}, \pi, \frac{3\pi}{2}\right]. \tag{2.47}$$

From Sec. 2.4, we already know that no spectrum exists along the Stokes lines; we have now established that this is directly connected to the non-normalizability of the wave function. The Stokes and anti-Stokes lines are

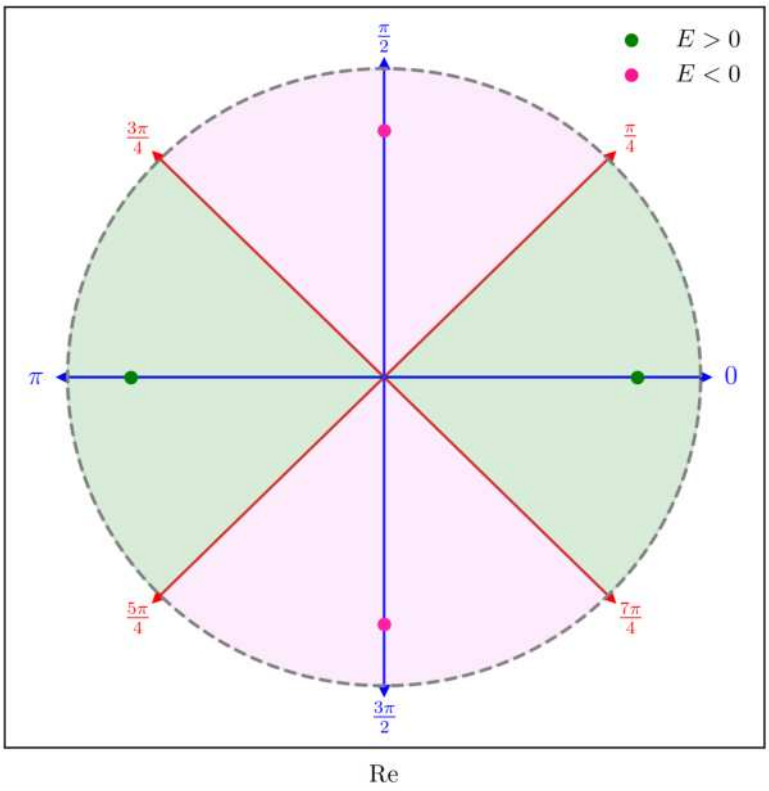

Figure 2.11: Stokes and anti-Stokes structure of the harmonic oscillator on the unit circle. The shaded regions represent sectors in which the real part of the exponent of the asymptotic wave function is negative, leading to decaying solutions, whereas the Stokes lines correspond to purely oscillatory behavior.

illustrated in Fig. 2.11. The area between two Stokes lines is called Stokes sector [7]. The jump between $+E_n$ and $-E_n$, shown in Fig. 2.1 can be understood by looking at the turning points of the system. Turning points are defined as the points where the potential equals the energy: $V(q) = E$. In the case of the transformed harmonic oscillator (2.39), these satisfy

$$q^2 e^{-2i\phi} = E. \tag{2.48}$$

In the following, we will focus only on real turning points. Solving for q gives

$$q \propto \sqrt{\pm e^{-2i\phi}} = \begin{cases} e^{-i\phi + k\pi} & E > 0 \\ e^{-i\phi + k\pi + \frac{\pi}{2}} & E < 0 \end{cases} \qquad k = 0, 1. \tag{2.49}$$

Requiring the turning points to lie on the real axis ($q \in \mathbb{R}$), yields the corresponding values of ϕ:

$$\phi = \begin{cases} [0, \pi] & E > 0 \\ \left[\frac{\pi}{2}, \frac{3\pi}{2}\right] & E < 0. \end{cases} \tag{2.50}$$

In Fig. 2.11, the turning points of the Hamiltonian are also shown. We observe that for the harmonic oscillator, they lie directly on the anti-Stokes lines.

Specifically, the turning points with $E < 0$ are located in the pink regions while those with $E > 0$ lie in the green region.

Comparing the behavior along the Stokes and anti-Stokes lines with the results obtained in the previous section leads to the conclusion that a well-defined spectrum exists everywhere except on the Stokes lines. Along these lines, the wave function exhibits oscillatory behavior for large q. This is connected to the non-existence of a physical spectrum. Since the asymptotic form of the wave function on the Stokes lines is not normalizable, an expansion in terms of Hermite functions is no longer meaningful. For the harmonic oscillator, the eigenvalues of the spectrum are real. As shown in Fig. 2.1, we observe that in the Stokes sectors containing a turning point with $E > 0$, the corresponding eigenvalues satisfy $E_n > 0$. Conversely, in Stokes sectors associated with a turning point at $E < 0$, the eigenvalues of the spectrum are negative. [3].

Using the example of the complex-deformed harmonic oscillator, we have gained insight into the conditions governing the existence and non-existence of spectra for this class of Hamiltonians. In the following chapter, we apply these insights to a more general class of Hamiltonians and analyze the corresponding spectra and wave-function solutions.

[3]To gain a deeper understanding of this behavior, a detailed discussion of $\mathcal{PT}-$-symmetry would be necessary. However, such an analysis lies beyond the scope of this thesis. We will come back to the discssion of turning points and stokes sectors in the subsequent chapter.

Chapter 3

Spectra of General Non-Hermitian Operators

In this chapter, we extend the analysis of the harmonic oscillator to a broader class of non-Hermitian Hamiltonians. We derive general expressions for the Stokes, anti-Stokes lines and turning points. In this context, we will discuss the existence of real and complex eigenvalues, calculated in the truncated Hermite basis.

3.1 Standardization of Non-Hermitian Operators

In this section, we will consider the general class of Hamiltonians of the form

$$H = p^2 + ipf(q) + g(q), \tag{3.1}$$

where q and p are the dimensionless position and momentum operator satisfying $[q, p] = i$ with $p = -i\frac{d}{dq}$. We now consider a transformation of the left and right eigenfunctions of the form $\Psi_R(q) = e^{h(q)}\psi_R(q)$ and $\Psi_L(q) = \psi_L(q)e^{-h(q)}$. Under this transformation square-integrabiltity remains, because

$$\int_{-\infty}^{\infty} dq\, \Psi_L^*(q)\Psi_R(q) = \int_{-\infty}^{\infty} dq\, \psi_L^*(q)e^{-h(q)}e^{h(q)}\psi_R(q) < \infty, \tag{3.2}$$

provided that $h(q)$ does not alter the asymptotic decay of the right eigenfunction. We can also examine how the operators transform under this map. For the position operator q, we have

$$e^{-h(q)}qe^{h(q)} = e^{-h(q)}e^{h(q)}q = q, \tag{3.3}$$

since q commutes with any function of itself $[q, f(q)] = 0$. For the momentum operator, we use the standard commutator relation $[p, h(q)] = -ih'(q)$ to obtain

$$e^{-h(q)}pe^{h(q)} = e^{-h(q)}\left(-i\frac{d}{dq}e^{h(q)} + e^{h(q)}p\right) = e^{-h(q)}e^{h(q)}\left(p - ih'(q)\right). \tag{3.4}$$

This shows that, under the transformation, the momentum operator effectively undergoes an additive shift proportional to the derivative of $h(q)$. The commutator relation still holds with

$$[q, p - ih'(q)] = [q, p] - i[q, h'(q)] = [q, p] = i. \tag{3.5}$$

Let us now apply the previous transformation of the wave function to the general Hamiltonian of Eq. (3.1). Then, the transformed Hamiltonian can be written as

$$\begin{aligned}\tilde{H} &= [p - ih'(q)]^2 + i[p - ih'(q)]f(q) + g(q) \\ &= p^2 - 2iph'(q) + h''(q) + ipf(q) + h'(q)f(q) + g(q) - h'(q)^2 \\ &= p^2 + ip[-2h'(q) + f(q)] + [h''(q) + h'(q)f(q) + g(q) - h'(q)^2] \\ &\stackrel{!}{=} \beta\,(p^2 + V(q)),\end{aligned} \tag{3.6}$$

where we have once more employed the commutator relation $[p, h(q)] = -ih'(q)$. In the last line of Eq. 3.6 we indicate our intention to express $\tilde{H}$ in the form of a standard Hamiltonian with potential $V(q)$. For this to hold, however, we must have $\beta = 1$ and

$$-2h'(q) + f(q) = 0 \Leftrightarrow h'(q) = \frac{1}{2}f(q). \tag{3.7}$$

The potential $V(q)$ then can be written in the form of

$$V(q) = \frac{1}{2}f'(q) + \frac{1}{4}f(q)^2 + g(q), \tag{3.8}$$

where we have used $h''(q) = \frac{1}{2}f'(q)$. By applying a transformation of the form $\tilde{\psi}_R(q) = \exp\left[\frac{1}{2}\int^q f(q')dq'\right]\psi_R(q)$, we thus can bring the Hamiltonian of Eq. (3.1) into a standardized form $\tilde{H} = p^2 + V(q)$. In the following, we restrict ourselves to polynomial functions, i.e. $f(q) \propto aq^n$ and $g(q) \propto bq^k$ with $a, b \in \mathbb{C}$ and $n, k \in \mathbb{N}$. In this case, the Hamiltonian can be standardized into a form of $H = \beta(p^2 + V(q))$, where $V(q) \propto \alpha q^n$.

In Ch. 2.1, we showed that for the harmonic oscillator, corresponding to the polynomial potential $V(q) = q^2$, the definition of a spectrum and the computation of eigenfunctions are possible everywhere except on the Stokes lines. In the present section, we have demonstrated that general non-Hermitian Hamiltonians of the form of Eq. (3.1) can be mapped to a standardized form with a polynomial potential. This mapping allows the spectral problem to be analyzed within the same framework. In the next section, we additionally formulate the Stokes and anti-Stokes lines for general polynomial potentials.

3.2 WKB-Approximation and Stokes Sectors

In Ch. 2.1, we showed that, in the case of the harmonic oscillator, the time-independent Schrödinger equation admits two asymptotic solutions for large q

behaving as $\psi(q) \propto \exp(\pm q^2/2)$. We now aim to generalize this asymptotic behavior to polynomial potentials of the form $V(q) \propto \gamma q^n$. To this end, we employ the semiclassical approximation for the one-dimensional time-independent Schrödinger equation (2.4) in the limit of large quantum numbers n, known as WKB-approximation. In the WKB approach, the wave function is written in exponential form as

$$\psi(q) = Ae^{iS(q)}, \tag{3.9}$$

where $S(q)$ is a rapidly varying function. In the present analysis, we restrict ourselves to the case of a constant amplitude A. The second derivative is given by

$$\frac{d^2}{dq^2}\psi(q) = \frac{d^2}{dq^2}Ae^{iS(q)} = iAS''(q)e^{iS(q)} - AS'(q)^2e^{iS(q)}. \tag{3.10}$$

Substituting this equation into the time-independent Schrödinger equation (2.4) and multiplying by $\frac{1}{A}e^{-iS(q)}$ yields

$$E = -iS''(q) + S'(q)^2 + V(q). \tag{3.11}$$

The WKB approximation is valid if $S(q)$ varies slowly, such that $S''(q) \ll S'(q)^2$. This results in the differential equation

$$S'(q) = \pm\sqrt{[E - V(q)]} = \pm p(q). \tag{3.12}$$

Therefore, the wave function can be written in the form of

$$\psi(q) = A_+ \exp\left(+i\int_{-\infty}^{\infty} pdq\right) + A_- \exp\left(-i\int_{-\infty}^{\infty} pdq\right), \tag{3.13}$$

with $p = \sqrt{E - V(q)}$.
In order, to be considered as part of the physical spectrum, the corresponding wave functions $\psi(q)$ must be normalizable, which requires that they decay sufficiently fast for large q, so that

$$\int_{-\infty}^{\infty} dq\,|\psi(q)|^2 < \infty. \tag{3.14}$$

Consequently, the coefficient of the non-decaying term in Eq. (3.13) are set to zero, leaving a wave function that decays asymptotically.

We now consider standardized Hamiltonians of the form

$$H = p^2 + \gamma q^n, \tag{3.15}$$

with $\gamma \in \mathbb{C}$. As in the case of the harmonic oscillator we apply the transformation of the form $p \to e^{i\phi}p$ and $q \to e^{-i\phi}q$ with $\phi \in [0, 2\pi)$. The transformed Hamiltonian then reads

$$H = p^2e^{2i\phi} + \gamma q^n e^{-ni\phi}. \tag{3.16}$$

We use the WKB approximation of Eq. (3.13), to determine for which angles ϕ decaying solutions exist and for which the wave function is purely oscillatory. Equation (3.12) can be written as

$$p^2 e^{2i\phi} + \gamma e^{-in\phi} = E \approx 0, \tag{3.17}$$

where, for simplicity, we have set the constant energy to zero. Solving for the squared momentum yields

$$p^2 = -\gamma e^{-i\phi(n+2)} q^n. \tag{3.18}$$

The constant γ is generally complex and can be written in polar form as $\gamma = r^{i\theta}$, where r denotes the modulus and θ the argument of the complex number. Taking the square root gives

$$p = \sqrt{-r q^n e^{i[\theta - \phi(n+2)]}} = i\sqrt{r} q^{n/2} e^{i\frac{\theta-(n+2)\phi}{2}}, \tag{3.19}$$

and the cooresponding WKB-approximated wave function, see Eq. (3.13), reads

$$\psi(q) \propto \exp\left(\pm\sqrt{\frac{r}{\alpha}} q^{n/2} e^{i\frac{\theta-(n+2)\phi}{2}}\right). \tag{3.20}$$

The Stokes lines are defined as the points where the wave function is purley oscillatory which occurs when

$$\begin{aligned} \exp\left(i\frac{\theta-(n+2)\phi}{2}\right) = \pm i \quad &\Leftrightarrow \quad \cos\left(\frac{\theta-(n+2)\phi}{2}\right) = 0 \\ \Rightarrow \frac{\theta}{2} - \frac{n+2}{2}\phi = \frac{2j+1}{2}\pi \quad &, j = 0, 1, 2, ..., n+1. \end{aligned} \tag{3.21}$$

Solving for ϕ yields the general calculation of the Stokes lines[1]

$$\phi_{st} = \frac{\theta - \pi(2j+1)}{n+2} + 2\pi. \tag{3.22}$$

Thus, a polynomial potential $V(q) \propto \gamma q^n$ has $n+2$ Stokes lines. The number is even for even n and odd for odd n.
The anti-Stokes lines are determined the same way. They occur when the exponent is real, i.e.,

$$\begin{aligned} e^{i\frac{\theta-(n+2)\phi}{2}} = \pm 1 \quad &\Leftrightarrow \quad \sin\left(\frac{\theta-(n+2)\phi}{2}\right) = 0 \\ \Rightarrow \frac{\theta}{2} - \frac{n+2}{2}\phi = j\pi \quad &, j = 0, 1, 2, .., n+1. \end{aligned} \tag{3.23}$$

Solving for ϕ yields the general calculation of the anti-Stokes lines

$$\phi_{ast} = \frac{\theta - 2j\pi}{n+2} + 2\pi. \tag{3.24}$$

[1]The addition of 2π is performed to ensure that the condition $\phi_{st} \in [0, 2\pi)$ is satisfied. However, for certain values of θ and ϕ_{st}, this addition may not be necessary. The same principle applies to calculating the anti-Stokes lines and turning points.

As for the Stokes lines, there are $n + 2$ anti-Stokes lines.

The turning points are defined as the points where $E = V(q)$. Focusing on real turning points ($E \in \mathbb{R}$), we have

$$E = V(q) = \gamma q^n e^{-in\phi} = rq^n e^{i(\theta - n\phi)}, \tag{3.25}$$

where we have, once again, used the polar representation $\gamma = re^{i\theta}$. Solving for q gives

$$q = \exp\left(i\frac{(-\theta + n\phi + 2\pi k)}{n}\right)\left(\frac{E}{r}\right)^{1/n}. \tag{3.26}$$

For $E > 0$, the turning points satisfy

$$-\theta + n\phi + 2\pi k = 0 \Leftrightarrow \phi = \frac{\theta - 2\pi k}{n}, \tag{3.27}$$

and for $E < 0$, they are given by

$$-\theta + n\phi + 2\pi k + \pi = 0 \Leftrightarrow \phi = \frac{\theta - (2k+1)\pi}{n}, \tag{3.28}$$

where we have used $e^{i\pi} = -1$. For general potentials of the form $V(q) = \gamma q^n$ we have thus determined the locations of the Stokes and anti-Stokes lines as well as the turning points. In the upcoming sections, we will discuss several illustrative examples of such potentials.

3.3 $H = p^2 + iq^3$

We now want to discuss the Hamiltonian of the form

$$H = p^2 + iq^3 \to p^2 e^{2i\phi} + iq^3 e^{-3i\phi}. \tag{3.29}$$

The potential can be written in the form of $V(q) = re^{i(\theta - n\phi)}q^n$ with $r = 1$, $\theta = \frac{\pi}{2}$ and $n = 3$. Substituting these values into the general expressions for the Stokes and anti-Stokes lines, see Eqs. (3.22) and (3.24), yields five lines in each case

$$\begin{aligned} \phi_{st} &= \left[\frac{3\pi}{10}, \frac{7\pi}{10}, \frac{11\pi}{10}, \frac{3\pi}{2}, \frac{19\pi}{10}\right] \\ \phi_{ast} &= \left[\frac{\pi}{10}, \frac{\pi}{2}, \frac{9\pi}{10}, \frac{13\pi}{10}, \frac{17\pi}{10}\right]. \end{aligned} \tag{3.30}$$

The turning points are given by

$$\phi_{turning} = \begin{cases} \left[\frac{\pi}{6}, \frac{5\pi}{6}, \frac{3\pi}{2}\right], E > 0 \\ \left[\frac{\pi}{2}, \frac{7\pi}{6}, \frac{11\pi}{6}\right], E < 0. \end{cases} \tag{3.31}$$

Figure 3.1 illustrates the Stokes and anti-Stokes structure of the iq^3-potential with the turning points indicated. Since $n = 3$ is odd, the total number of

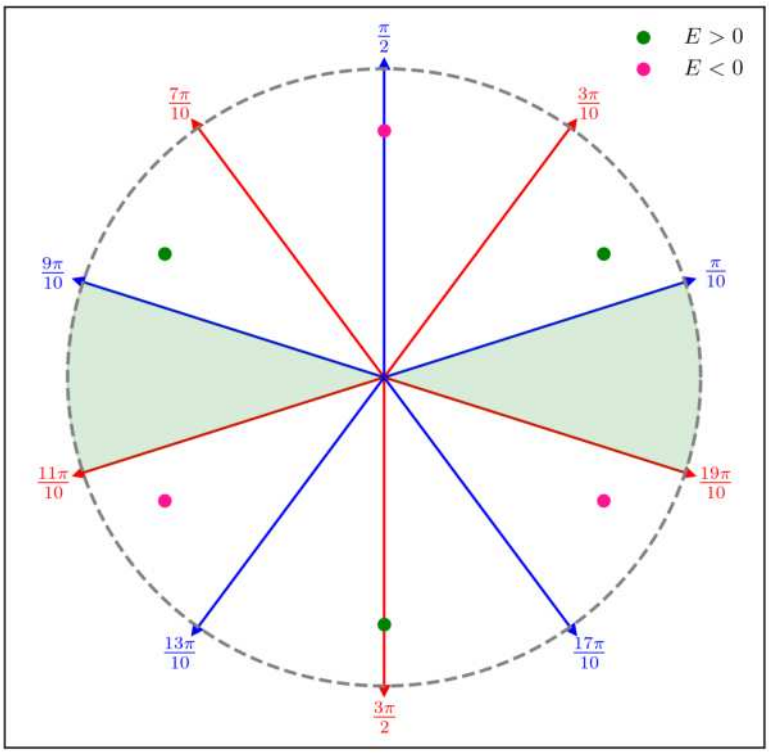

Figure 3.1: Stokes and anti-Stokes structure of the iq^3-potential on the unit circle. The green regions represent the region in which spectra with energy values $E_n \in \mathbb{R}$ are found.

Stokes and anti-Stokes lines, $n + 2 = 5$ is also odd. Consequently, each anti-Stokes line lies opposite to a Stokes line. Turning points are located between two Stokes lines, and in each Stokes sector, exactly one real turning point is present.

The eigenvalues and eigenvectors of the Hamiltonian of Eq. (3.29) are computed following the same procedure as for the harmonic oscillator. The calculation is performed in the basis of Hermite functions, truncated at a cutoff N. The resulting eigenvalues E_n are sorted according to their absolute value. Figure 3.2 shows the computed eigenvalues as a function of the angle ϕ. In contrast to the harmonic oscillator (Fig. 2.1), most eigenvalues are complex. Real eigenvalues occur only within the intervals $\phi \in \left(-\frac{\pi}{10}, \frac{\pi}{10}\right)$ and $\phi \in \left(\frac{9\pi}{10}, \frac{11\pi}{10}\right)$. Apparent discontinuities appear at $\phi = \frac{(2k+1)\pi}{10}$ with $k = 0, 1, 2, ...$ At higher eigenvalues such as E_7 and E_{10}, the corresponding transitions become increasingly less steep. This reduces the intervals of ϕ over which the eigenvalues remain approximately constant.

From the harmonic-oscillator example we know that these discontinuities occur at the Stokes lines, and that their apparent smoothing is a numerical artifact

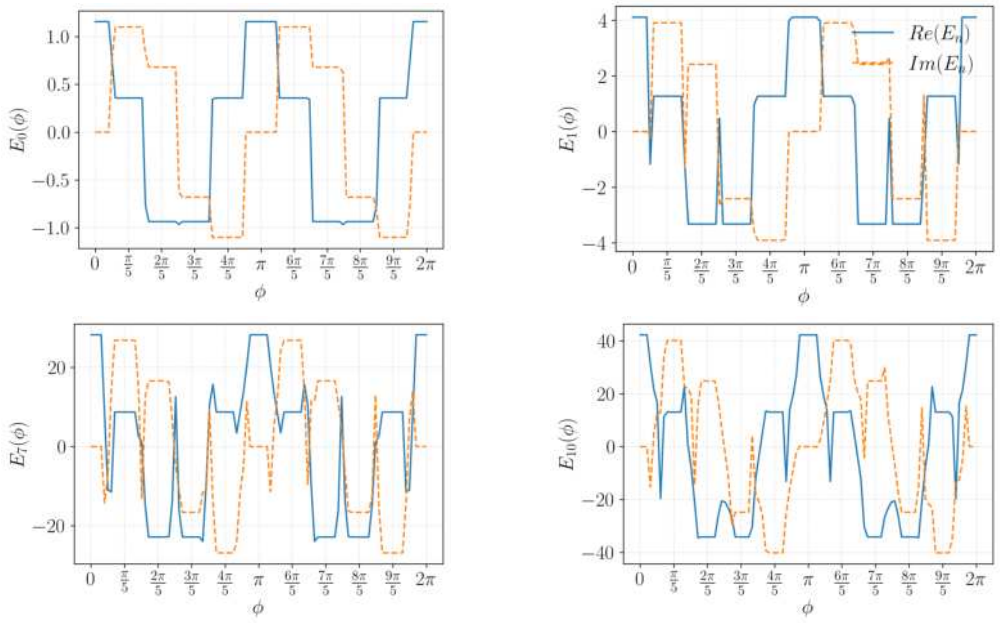

Figure 3.2: E_0, E_1, E_7 and E_{10} of the iq^3-potential plotted as functions of the angle ϕ for $N = 200$. Sharp transitions appear on the Stokes- and anti-Stokes lines. Due to the cutoff of the Hermite basis, with increasing basis index i, the sharp lines are increasingly less steep. Around $\phi = 0$ and $\phi = \pi$, the eigenvalues are real.

resulting from the truncation of the Hermite basis. Eigenvalues near the Stokes lines are particularly sensitive to this cutoff, which reduces the number of eigenvalues that can be reliably regarded as part of the physical spectrum compared to regions farther from the Stokes lines.
For the iq^3-potential, such discontinuities appear not only on the Stokes lines but also on the anti-Stokes lines. As shown in Fig. 3.1, the Stokes and anti-Stokes lines lie opposite to each other. Consequently, the behavior along the anti-Stokes lines mirrors that along the Stokes lines. Given that, the eigenvalues of Eq. (3.29) are no longer entirely real, it remains necessary to determine which eigenvalues can be considered part of the spectrum and which cannot.

Figure 3.3 shows the tail-weight ratio y, plotted as a function of the basis cutoff N. Shown are four different angles in the first stokes sector: $\phi = 0$, $\phi = \frac{\pi}{10}$ on the first anti-Stokes line, $\phi = \frac{3\pi}{20}$ and $\phi = \frac{3\pi}{10}$ on the first Stokes line. No significant differences in the tail-weight ratios are observed between these angles. This indicates that the first ten eigenvectors are localized in the low-index region of the Hermite basis, and that y_n converges reliably both on and off the Stokes lines.

For a more quantitative evaluation, Fig. 3.4 shows the truncation fidelity z as a function of the cutoff N, plotted for the same angles as in Fig. 3.3. Within

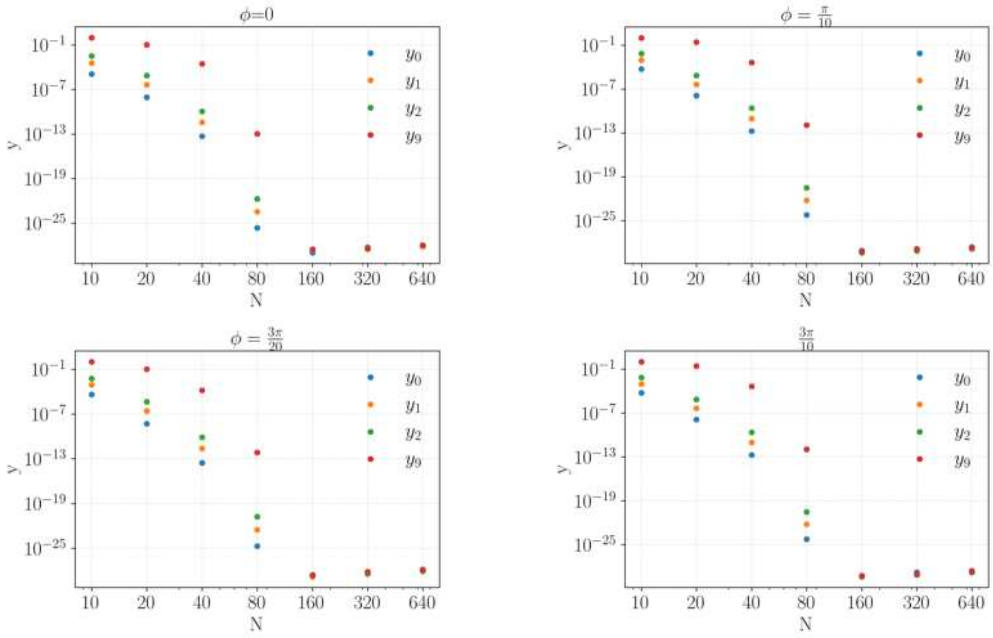

Figure 3.3: Tail-weight ratio of the iq^3-potential for different cutoff values N, evaluated for $\phi = 0, \phi = \frac{\pi}{10}, \phi = \frac{3\pi}{20}$ and $\phi = \frac{3\pi}{10}$.

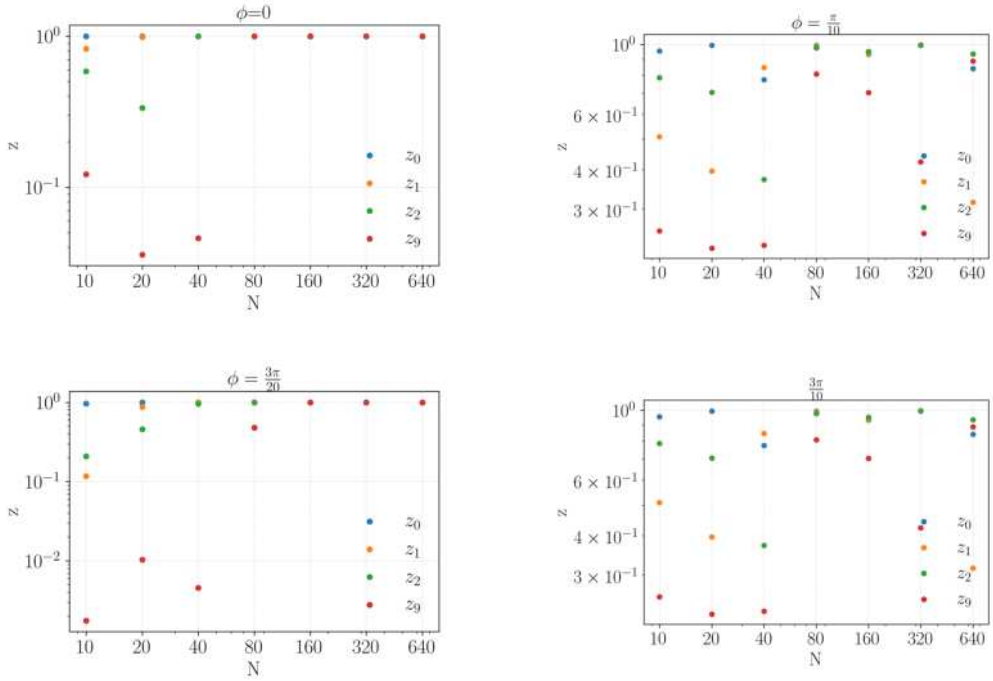

Figure 3.4: Truncation fidelity for different cutoff values N, evaluated for angles ϕ around and exactly on the first Stokes line and anti-stokes line. The first ten eigenvectors are localized in the low-index region of the basis and y_n converges reliably.

the Stokes sector ($\phi = 0$ and $\phi = \frac{3\pi}{20}$) z appears to converge to unity, indicating that increasing the basis size yields essentially the same eigenvectors. However, for the iq^3-potential z, does not converge on the Stokes line $\phi = \frac{3\pi}{10}$. Moreover, even on the anti-Stokes line $\phi = \frac{\pi}{10}$ where the WKB-approximated wave function exhibits purely decaying behavior, no significant convergence of the truncation fidelity is observed.

These results are consistent with the observations shown in Figs. 3.1 and 3.2. The anti-Stokes lines effectively act as Stokes lines because they lie opposite to them. Away from these lines, a set of eigenvalues can be identified that can be regarded as part of the spectrum, even though these eigenvalues are not necessarily real. A group of spectral regions with real eigenvalues $E_n > 0$ is found around the real axis, within an angular range $\Delta\phi = \pm\pi/10$. This behavior can be understood in terms of the turning points of the system. Within the green region of Fig. 3.1, it is possible to draw a straight line connecting one Stokes sector containing a positive turning point to another Stokes sector containing a positive turning point. Consequently, the eigenvalues are real and positive within this region. [2]

In summary, the analysis of the iq^3-potential yields the expected results. Along the unit circle, well-defined spectral regions can be identified everywhere except on the Stokes lines.

3.4 $H = p^2 + q^6$

Let us now consider the Hamiltonian of the form

$$H = p^2 + q^6 \;\rightarrow\; p^2 e^{2i\phi} + q^6 e^{-6i\phi}. \tag{3.32}$$

In this case the potential $V(q) = q^6$ is of the form $e^{i\theta} q^n$ with $\theta = 0$ and $n = 6$. Substituting into Eqs. (3.22) and (3.24) yields eight Stokes and eight anti-Stokes lines located at

$$\begin{aligned} \phi_{st} &= \left[\frac{\pi}{8}, \frac{3\pi}{8}, \frac{5\pi}{8}, \frac{7\pi}{8}, \frac{9\pi}{8}, \frac{11\pi}{8}, \frac{13\pi}{8}, \frac{15\pi}{8}\right] \\ \phi_{ast} &= \left[0, \frac{\pi}{4}, \frac{\pi}{2}, \frac{3\pi}{4}, \pi, \frac{5\pi}{4}, \frac{3\pi}{2}, \frac{7\pi}{4}\right]. \end{aligned} \tag{3.33}$$

[2] One may ask why no negative real spectrum is found within the angular intervals $\phi = \left[\frac{\pi}{2}, \frac{7\pi}{10}\right]$ and $\phi = \left[\frac{3\pi}{2}, \frac{17\pi}{10}\right]$. In these intervals, it is also possible to draw a straight line connecting one Stokes sector containing a negative turning point to another Stokes sector containing a negative turning point. Following the argument above, one would therefore expect the eigenvalues in this region to be real with $E_n < 0$. However, Fig. 3.2 shows that this is not the case. Addressing this question requires a detailed discussion of $\mathcal{PT}$-symmetry which is beyond the scope of this thesis. Briefly, the spectrum of non-Hermitian operators with $\mathcal{PT}$-symmetry are entirely real [3]. For the iq^3-potential potential, this symmetry is realized around the real axis [3, 7].

The turning points follow from Eq. (3.28) and are given by

$$\phi_{turning} = \begin{cases} \left[0, \frac{\pi}{3}, \frac{2\pi}{3}, \pi, \frac{4\pi}{3}, \frac{5\pi}{3}\right] , E > 0 \\ \left[\frac{\pi}{6}, \frac{\pi}{2}, \frac{5\pi}{6}, \frac{7\pi}{6}, \frac{3\pi}{2}, \frac{11\pi}{6}\right] , E < 0. \end{cases} \tag{3.34}$$

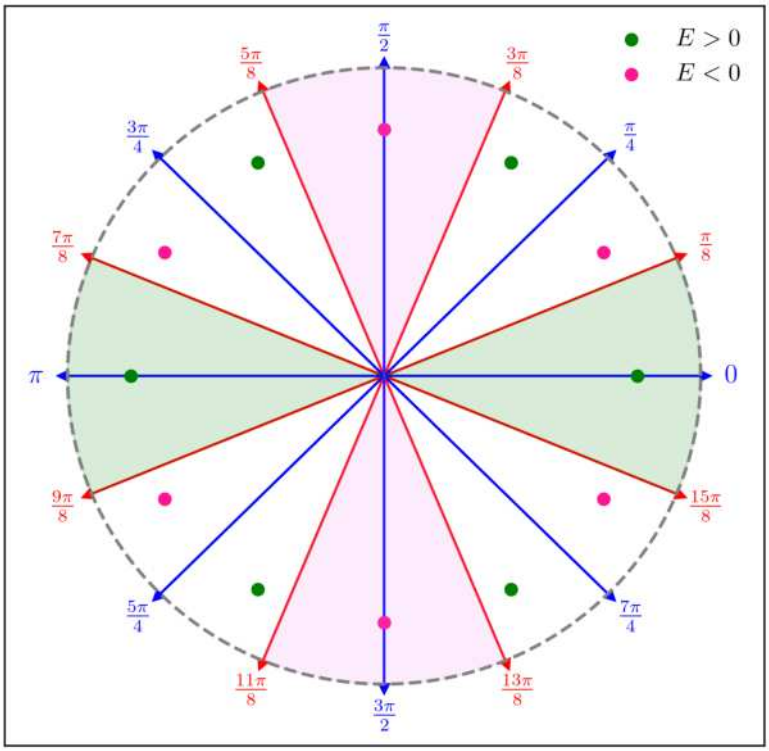

Figure 3.5: Stokes and anti-Stokes structure of the q^6-potential along the unit circle. Turning points with positive energy are marked in green, while turning points with negative energy are marked in pink. In the green regions, a positive spectrum is found, whereas in the pink regions the eigenvalues are negative. In all other regions, which contain two turning points of opposite sign, the eigenvalues are complex with $Re(E_n) = 0$.

Figure 3.5 illustrates the Stokes- and anti-Stokes structure of the sextic potential. The location of the turning points is also specified. Since $n = 6$ is even, the number of Stokes and anti-Stokes lines is also even, and consequently each Stokes line lies opposite to another Stokes line. This example exhibits four Stokes sectors containing two turning points of opposite sign, as well as four Stokes sectors that contain only a single turning point. In the Stokes sectors $\left[-\frac{\pi}{8}, \frac{\pi}{8}\right]$ and $\left[\frac{7\pi}{8}, \frac{9\pi}{8}\right]$ only a single real positive turning point exists, whereas in the sectors $\left[3\frac{\pi}{8}, \frac{5\pi}{8}\right]$ and $\left[\frac{11\pi}{8}, \frac{13\pi}{8}\right]$ only a single real negative turning point occurs.

Figure 3.6 shows the behavior of the ground state energy as a function of ϕ.

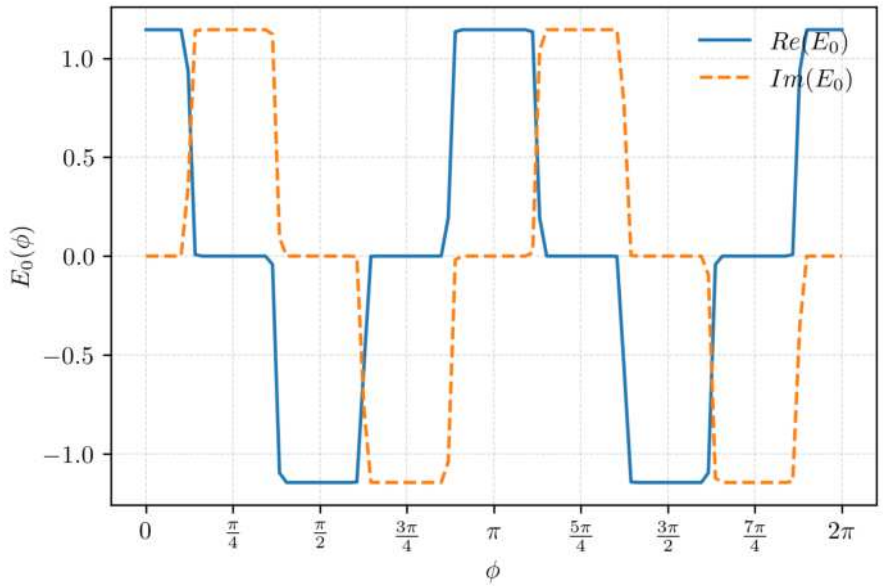

Figure 3.6: Ground state energy of the q^6-potential as a function of the angle ϕ.

In the cases of the harmonic oscillator (Sec. 2.2) and the cubic potential (Sec. 3.3), we have already discussed how this behavior changes numerically for higher states, due to the cutoff of the basis. The same considerations apply to the q^6-potential. Therefore, this case will not be discussed further. The structure of $E_0(\phi)$ is in agreement with the Stokes structure, shown in Fig. 3.5. Discontinuities appear on the Stokes lines. In the green sectors, which contain one turning point with $E > 0$, the eigenvalues are real and positive. In contrast, in the pink sectors, which contain a real turning point with $E < 0$, the eigenvalues are real and negative. In the sectors with two turning points, the energy is purely imaginary.

Figure 3.7 shows the tail-weight-ratio and truncation fidelity for two different values of ϕ. For $\phi = 0$, which lies in the first Stokes sector, y_n and z_n exhibit significant convergence for cutoff values $N > 320$. On the Stokes-line $\phi = \frac{\pi}{8}$, however, the truncation fidelity does not fully converge to unity. Consequently, the corresponding eigenvalues E_n can not be considered as part of the spectrum. A meaningful definition of the spectrum on the Stokes line is not possible. This observation is once again fully consistent with the theoretical expectation that the spectrum is well-defined under rotations of the form given in Eq. (2.37), except on the Stokes lines.

This behavior can be observed for a wide class of Hamiltonians of the form $H \propto \gamma q^n$ and always leads to the same conclusion. For potentials $V(q) = -q^4$ and $V(q) = -iq^5$ Figures illustrating the Stokes structure and plots of the ground-state energy $E_0(\phi)$ are provided in the appendix (see Figs. 7, 8, 9 and

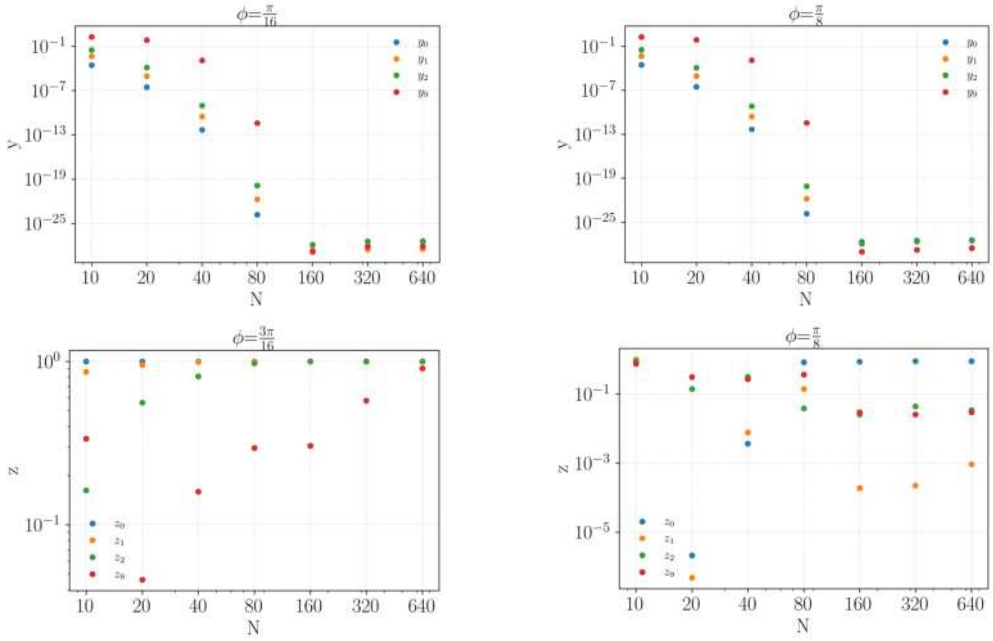

Figure 3.7: Tail-weight-ratio y_n and truncation fidelity z_n in dependence on the basis cutoff N. Shown are the first four states for $\phi = \frac{\pi}{16}$ and on the Stokes line $\phi = \frac{\pi}{8}$.

10). In some sectors of non-Hermitian Hamiltonians, it is even possible to define a real spectrum. This appears to depend on the arrangement of the turning points within the sector. Sectors that contain a single real turning point and lie opposite another sector with a single real turning point of the same sign seem to support a spectrum with real eigenvalues, despite the Hamiltonian being non-Hermitian. In the Figures showing the Stokes and anti-Stokes structure of the potentials considered here (see Fig. 2.11, 3.1 and 3.5), these sectors are marked in green for positive turning points and pink for negative turning points. However a detailed interpretation of this behavior requires a discussion of $\mathcal{PT}$-symmetric Hamiltonians [7].

3.5 $H = p^2 \pm ipq^3$

Let us now consider the Hamiltonian of the form

$$H = p^2 + ip(\beta q - q^3) = p^2 + ipf(q), \tag{3.35}$$

with $f(q) = \beta q - q^3$ and $\beta \in \mathbb{C}$. In Sec. 3.1 we have shown that by applying a transformation of the form $\exp(h(q))\psi_R(q)$ or $p \to p - ih'(q)$, we can rewrite this problem into a standardized problem of the form $V(q) \propto \gamma q^n$. Substituting $f(q)$ into Eq. (3.8) yields

$$V(q) = \frac{1}{2}\left(\beta - \left[3 - \frac{\beta^2}{2}\right] q^2 - \beta q^4 + \frac{1}{2}q^6\right). \tag{3.36}$$

We consider the case $\beta = 0$, for which the potential reduces to

$$V_-(q) = \frac{1}{2}\left(-3q^2 + \frac{q^6}{2}\right). \tag{3.37}$$

Since the position operator q is Hermitian, all integer powers of q are also Hermitian

$$(q^n)^\dagger = (q^\dagger)^n = q^n. \tag{3.38}$$

Consequently, the resulting Hamiltonian $H = p^2 + V(q)$ is Hermitian. We have thus transformed the non-Hermitian Hamiltonian of Eq. (3.35) into a, in this example, Hermitian form. The eigenfunctions and eigenvalues of the Hamiltonian with the potential given in Eq. (3.37), as well as of the non-standardized Hamiltonian in Eq. (3.35), can be computed using Hermite functions as a basis. Figure 3.8 shows the calculated spectrum for both the standardized and

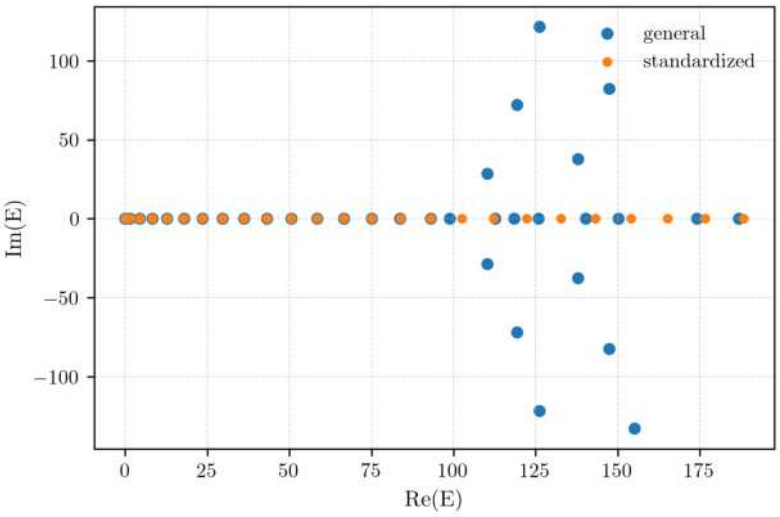

Figure 3.8: Spectrum of the standardized and the general Hamiltonian of basis size $N = 320$. For eigenvalues within the stable part of the spectrum, the eigenvalues of both Hamiltonians coincide.

the general Hamiltonian with a basis size $N = 320$. In the general case, the Hamiltonian is non-Hermitian, which leads to numerical instabilities in the eigenvalues for large quantum numbers n. For these high-energy states, the eigenvalues of the general and the standardized Hamiltonian do not coincide. Nevertheless, for states that are not influenced by the cutoff of the Hermite basis, the eigenvalues E_n of both Hamiltonians agree. This demonstrates that the standardization procedure preserves the spectrum, yielding identical eigenvalues.

Now, we want to look at the Hamiltonian of the form

$$H = p^2 + ipq^3 \tag{3.39}$$

and compare it with the negative case discussed above. Applying the standardization procedure using Eq. (3.8) yields the potential

$$V_+(q) = \frac{1}{2}\left(3q^2 + \frac{q^6}{2}\right), \tag{3.40}$$

which again gives a Hermitian Hamiltonian. Calculating the eigenvalues of this Hamiltonian in a truncated basis of Hermite functions gives the first ten quantum states, shown in Tab. 3.1. In comparison, Tab. 3.2 shows the eigenvalues obtained for the negative case ($p^2 - ipq^3$), , which, as discussed above, coincide in both the general and standardized forms. In case of Tab. 3.1, the ground state of the standardized problem is missing.

	$p^2 + ipq^3$	$p^2 + V_+(q)$
E_0	0	1.368593
E_1	1.368593	4.453709
E_2	4.453709	8.259694
E_3	8.259694	12.758070
E_4	12.758070	17.857702
E_5	17.857702	23.494408
E_6	23.494409	29.621418
E_7	29.621417	36.202388
E_8	36.202419	43.208015
E_9	43.208014	50.614022

Table 3.1: Comparison of the first ten eigenenergys calculated in the truncated Hermite basis, in the general version standardized version, for $N = 320$. In the standardized case, the ground state is missing.

	$p^2 - ipq^3$	$p^2 + V_-(q)$
E_0	0	0
E_1	1.368593	1.368593
E_2	4.453709	4.453709
E_3	8.259694	8.259694
E_4	12.758070	12.758070
E_5	17.857702	17.857702
E_6	23.494409	23.494408
E_7	29.621417	29.621418
E_8	36.202419	36.202388
E_9	43.208014	43.208015

Table 3.2: Comparison of the first ten eigenenergys calculated in the truncated Hermite basis, in the general version standardized version, for $N = 320$. The eigenvalues completeley coincide.

The absence of the ground state in Table 3.1 can be understood from the structure of the Hamiltonian. The left eigenfunction of the ground state is given by

$$\begin{aligned} H^\dagger \psi_L(q) &= \left(p^2 \pm ipq^3\right)^\dagger \psi_L(q) \\ &= \left(p^2 \mp iq^3 p\right) \psi_L(q) \\ &= \left(-\frac{d^2}{dq^2} \mp q^3 \frac{d}{dq}\right) \psi_L(q) = 0 \\ &\Rightarrow \psi_L(q) = 1, \end{aligned} \tag{3.41}$$

where we have used $p^\dagger = p$,$q^\dagger = q$ and $(pq^3)^\dagger = q^3 p$. For zero-energy mode, the corresponding right eigenfunction of $p^2 - ipq^3$ is

$$\psi_R(q) \propto \exp(-\frac{q^4}{8}), \tag{3.42}$$

where we have used $h'(q) = f(q)/2$ from Sec. 3.1. In this case, square-integrability still holds because

$$\int_{-\infty}^{\infty} dq\, \psi_L^*(q)\psi_R(q) = \int_{-\infty}^{\infty} dq\, e^{-q^4/8} < \infty. \tag{3.43}$$

In contrast for $H = p^2 + ipq^3$, the right eigenfunction is

$$\psi_R(q) \propto \exp\left(\frac{q^4}{8}\right), \tag{3.44}$$

which is no longer square-integrable. Consequently, the ground state does not belong to the Hilbert space L^2 on which the standardized Hamiltonian $H = p^2 + V_+(q)$ is defined. Although the eigenvalue equation $H\psi_R(q) = 0$ is formally satisfied, the corresponding eigenfunction fails to meet the required boundary conditions. The ground state is therefore excluded from the physical spectrum. Despite not belonging to the physical Hilbert space, the zero eigenvalue can still appear in numerical calculations performed using a truncated Hermite basis. Consequently, when applying the standardization procedure, it is essential to carefully examine the resulting eigenstates with respect to boundary conditions and normalizability. In particular, the existence of a formally exact eigenvalue does not guarantee that the corresponding eigenstate lies within the physical Hilbert space.

Chapter 4

Conclusion and outlook

In this thesis, we investigated the properties and spectral behavior of several non-Hermitian quantum systems. The primary aim was to understand how non-Hermiticity affects eigenvalues, eigenfunctions, and the existence of physical spectra. We therefore developed a numerical framework to analyze these effects using a truncated Hermite basis. This allowed us to compute eigenvalues and eigenfuncions and discuss their stability.
We studied Hamiltonians of the form $H = p^2 + V(q)$ with $V(q) \propto \gamma q^n$ for large q under a complex deformation. Computing eigenfunctions and spectra in the truncated Hermite basis led to the appearance of spurious eigenvalues and non-converging eigenfunctions, which arise due to the cutoff of the Hermite basis. To distinguish physically meaningful eigenvalues from spurious ones, we introduced two quantitative measures: the tail-weight-ratio and the truncation fidelity. These quantities provide a practical criterion to test whether an eigenvalue can be considered part of the spectrum. By comparing their behavior with the asymptotic properties of the wave functions, we were able to identify regions with existing spectra.
Analyzing the asymptotic behavior of the wave functions in terms of Stokes and anti-Stokes lines showed that a spectrum exists in all sectors except on the Stokes lines themselves. Furthermore, a real spectrum can be identified in Stokes sectors containing a single real turning point that lie opposite a sector with a real turning point of the same sign[1].
We then extended this analysis to a broader class of non-Hermitian Hamiltonians of the form $H = p^2 + ipf(q) + g(q)$ and showed that, by introducing a suitable transformation, these problems can be brought into a standardized form $H = p^2 + V(q)$. For these systems, spectral existence is ensured everywhere except on the Stokes lines, allowing their spectra to be interpreted reliably. In particular, the eigenvalues of both Hamiltonians remain identical provided that the corresponding eigenfunctions belong to the Hilbert space of square-integrable functions.

An aspect that could be discussed further is the role of $\mathcal{PT}$-symmetry in relation to turning points and the structure of Stokes and anti-Stokes sectors.

[1] When $\mathcal{PT}$-symmetry is fullfilled [7].

While $\mathcal{PT}$-symmetry was not explicitly analyzed in this thesis, it is known to play an important role in the occurence of real spectra in certain non-Hermitian systems [3, 7]. A more detailed discussion of the existence of real and complex turning points within Stokes sectors, and of the connection between these occurrences, $\mathcal{PT}$-symmetry and the emergence of real or complex spectra, could therefore be undertaken. Also, in this thesis, only linear point transformations corresponding to straight integration axes were considered. Generalizing the transformations within the unit circle could lead to different integration contours that connect the Stokes sectors. This discussion could reveal real or complex spectral structures, depending on the turning points within the connected Stokes sectors.

Appendix

.1 Inverse Gaussian Integral Operator and Canonical Transformations

The kernel

$$K(q,q') = \exp\left(\alpha q^2 + \beta q'^2 + i\gamma q q'\right), \tag{.1}$$

with $\alpha, \beta, \gamma \in \mathbb{R}$ that defines a linear integral operator acting on functions in position space. Its action on a function f is given by

$$f' := (Tf)(q) = \int_{-\infty}^{\infty} dq'\, f(q') K(q,q'). \tag{.2}$$

$K(q,q')$ is assumed to be invertible in the sense of integral operators. Its inverse $K^{-1}(q,q')$ is defined through

$$\int_{-\infty}^{\infty} dq'\, K^{-1}(q'',q') K(q',q) = \delta(q''-q), \tag{.3}$$

where $\delta(q''-q)$ denotes the Dirac delta distribution. In order to determine the explicit form of the inverse kernel, we make the Gaussian ansatz

$$K^{-1}(q'',q') = N \exp\left(-[Aq''^2 - Bq'^2 - Cq''q']\right), \tag{.4}$$

with $A, B, C, N \in \mathbb{C}$. Substituting this ansatz into Eq. (.3) yields

$$\begin{aligned}\int_{-\infty}^{\infty} dq'\, K^{-1}(q'',q') K(q',q) &= N e^{-Aq''^2+\beta q^2} \int_{-\infty}^{\infty} dq'\, e^{-(B-\alpha)q'^2 - (Cq''-i\gamma q)q'} \\ &= N e^{-Aq''^2+\beta q^2} \sqrt{\frac{\pi}{B-\alpha}} \exp\left(\beta q^2 - Aq''^2 + \frac{(Cq''-i\gamma q)^2}{4(B-\alpha)}\right),\end{aligned} \tag{.5}$$

where the stndard Gaussian Integral

$$\int_{-\infty}^{\infty} dq\, e^{-(aq^2-bq+c)} = \frac{\pi}{a} e^{\frac{b^2}{4a}-c},$$

has been used. Since the right-hand side of Eq. (.3) is a Dirac delta distribution, it is convenient to express $\delta(q''-q)$ as the limit of a normalized Gaussian

$$\delta(q''-q) = \lim_{\varepsilon\to 0} \frac{1}{\sqrt{2\pi\varepsilon^2}} e^{-\frac{(q''-q)^2}{2\varepsilon^2}}. \tag{.6}$$

This allows for a direct comparison of the exponential terms in Eq. (.5) with the delta distribution. The exponent must therefore satisfy

$$\beta q^2 - Aq''^2 + \frac{1}{4(B-\alpha)}(C^2 q''^2 - 2iC\gamma q'' q - \gamma^2 q^2) = \lim_{\varepsilon\to 0} -\frac{1}{2\varepsilon^2}(q''^2 - 2qq'' + q^2). \tag{.7}$$

Comparing coefficients of q^2, q''^2, and qq'' yields three equations for the parameters A, B, and C:

$$\left(\beta - \frac{\gamma^2}{4(B-\alpha)}\right) = \lim_{\varepsilon\to 0} -\frac{1}{2\varepsilon^2} \tag{.8}$$

$$-\frac{iC\gamma}{2(B-\alpha)} = \lim_{\varepsilon\to 0} \frac{1}{\varepsilon^2} \tag{.9}$$

$$-A + \frac{C^2}{4(B-\alpha)} = \lim_{\varepsilon\to 0} -\frac{1}{2\varepsilon^2}. \tag{.10}$$

Solving these equations gives

$$A = \frac{\beta}{2\beta\varepsilon^2 + 1} \xrightarrow{\varepsilon\to 0} \beta \tag{.11}$$

$$B = \alpha + \frac{\varepsilon^2\gamma^2}{4\beta\varepsilon^2 + 2} \xrightarrow{\varepsilon\to 0} \alpha + 0^+ \tag{.12}$$

$$C = \frac{i\gamma}{2\varepsilon^2 + 1} \xrightarrow{\varepsilon\to 0} i\gamma. \tag{.13}$$

The normalization factor N is determined by imposing

$$\begin{aligned} 1 &= \int_{-\infty}^{\infty} dq\, \delta(q'' - q) = N\sqrt{\frac{\pi}{B-\alpha}} \int_{-\infty}^{\infty} dq\, e^{-\frac{1}{2\varepsilon^2}(q''-q)^2} \\ &= N\sqrt{\frac{\pi}{B-\alpha}} e^{-\frac{1}{2\varepsilon^2}q''^2} \sqrt{\frac{\pi}{1/2\varepsilon^2}} e^{\frac{1}{2\varepsilon^2}q''^2} = N\pi\sqrt{\frac{2\varepsilon^2}{B-\alpha}}. \end{aligned} \tag{.14}$$

Solving for N gives

$$N = \frac{\gamma}{2\pi}\sqrt{\frac{1}{2\varepsilon^2 + 1}} \xrightarrow{\varepsilon\to 0} \frac{\gamma}{2\pi}. \tag{.15}$$

Collecting all results, the inverse kernel is

$$K^{-1}(q, q'') = \frac{\gamma}{2\pi} \exp\left(-\beta q^2 - (\alpha + 0^+)q''^2 - i\gamma q q''\right). \tag{.16}$$

We now determine the effect of K and K^{-1} on the canonical variables p and q. Starting with the position operator, the transformed operator is given by

$$\begin{aligned} \hat{q}'(q, q') &= \int_{-\infty}^{\infty} dq''\, K^{-1}(q, q'') q'' K(q'', q') \\ &= \frac{\gamma}{2\pi} e^{-\beta(q^2 - q'^2)} \int_{-\infty}^{\infty} dq''\, q'' e^{-0^+ q''^2 + i\gamma(q'-q)q''} \\ &= \frac{i\gamma^2}{4}\sqrt{\frac{1}{\pi(0^+)^3}}(q' - q) e^{-\beta(q^2 - q'^2)} e^{-\frac{\gamma^2(q'-q)^2}{40^+}}. \end{aligned} \tag{.17}$$

Expanding the function $f(q') = \exp(-\beta(q^2 - q'^2))$ around $q' = q$ up to second order yields

$$(Tf)(q,q') = 1 - 2\beta q(q'-q) + \frac{1}{2}(-2\beta + 4\beta^2 q^2)(q'-q)^2 + ... \tag{.18}$$

The action on a wave function $\psi(q)$ is defined by

$$(\hat{q'}\psi)(q) = \int_{-\infty}^{\infty} dq'\, \hat{q'}(q,q')\psi(q'). \tag{.19}$$

Substituting the Taylor expansion of $f(q')$ yields

$$\begin{aligned}(\hat{q'}\psi)(q) = \frac{i\gamma^2}{4}\sqrt{\frac{1}{\pi(0^+)^3}}\int_{-\infty}^{\infty} dq'\,\psi(q')\, e^{-\frac{\gamma^2(q-q')^2}{40^+}}(q'-q) \\ \times\Big[1 - 2\beta q(q'-q) + (2\beta q^2 - \beta)(q'-q)^2 + ...\Big].\end{aligned} \tag{.20}$$

The integrals appearing are of the form

$$I := (0^+)^{-3/2}\int_{-\infty}^{\infty} dq'\psi(q')(q'-q)^m e^{-\frac{\gamma^2(q'-q)^2}{40^+}}.$$

and one can analyze for which powers m the prefactor $(0^+)^{-3/2}$ leads to a vanishing contribution as $0^+ \to 0$.

$$\begin{aligned}I &= (0^+)^{-3/2}\left(-\frac{20^+}{\gamma^2}\int_{-\infty}^{\infty} dq'\,\frac{(-\gamma^2)}{20^+}(q'-q)e^{-\frac{\gamma^2(q'-q)^2}{40^+}}(q'-q)^{m-1}\psi(q')\right) \\ &= -\frac{(0^+)^{-1/2}}{\gamma^2}\Big(\Big[(q'-q)^{m-1}e^{-\frac{\gamma^2(q'-q)^2}{40^+}}\psi(q')\Big]_{-\infty}^{\infty} \\ &\quad - \int_{-\infty}^{\infty} dq'\, e^{-\frac{\gamma^2(q'-q)^2}{40^+}}\frac{d}{dq'}\left[(q'-q)^{m-1}\psi(q')\right]\Big).\end{aligned} \tag{.21}$$

Performing partial integration and expanding $\psi(q')$ in a Taylor series

$$\psi(q') = \psi(q) + \psi'(q)(q'-q) + \frac{1}{2}\psi''(q)(q'-q)^2 + ..., \tag{.22}$$

shows that all higher-order terms vanish in the limit $0^+ \to 0$. Consequently, only the lowest-order contributions survive. Performing the derivation in I yields

$$\begin{aligned}I &= \frac{2(0^+)^{-1/2}}{\gamma^2}\Big((m-1)\int_{-\infty}^{\infty} dq'\,(q'-q)^{m-2}e^{-\frac{\gamma^2(q'-q)^2}{40^+}}\psi(q') \\ &\quad + \int_{-\infty}^{\infty} dq'\, e^{-\frac{\gamma^2(q'-q)^2}{40^+}}(q'-q)^{m-1}\psi'(q')\Big) \\ &= \frac{2(0^+)^{-1/2}}{\gamma^2}\Big(\frac{20^+}{\gamma^2}(m-1)\int_{-\infty}^{\infty} dq'\, e^{-\frac{\gamma^2(q'-q)^2}{40^+}}\frac{d}{dq'}[(q-q')^{m-3}\psi(q')] \\ &\quad + \int_{-\infty}^{\infty} dq'\, e^{-\frac{\gamma^2(q'-q)^2}{40^+}}(q-q')m-1[\psi'(q) + (q'-q)\psi''(q'=q) + ...)]\Big),\end{aligned} \tag{.23}$$

where we have used the Taylor expansion of $\psi'(q')$ around $q' = q$. After the second partial integration (if $m \geq 2$), each term acquires an additional factor of $(0^+)^{1/2}$. Therefore, all terms with $m \geq 2$ vanish in the limit $0^+ \to 0$, leaving only the lowest-order contributions. Consequently, the only integral terms of Eq. (.20) that survive in the limit $0^+ \to 0$ are

$$\begin{aligned}
\hat{q}'(q,q') &= \frac{i\gamma^2}{4}\sqrt{\frac{1}{\pi(0^+)^3}}\Big(\int_{-\infty}^{\infty} dq'\,\psi(q')\,e^{-\frac{\gamma^2(q-q')^2}{40^+}}(q'-q) \\
&\quad - 2\beta q\int_{-\infty}^{\infty} dq'\,\psi(q')\,e^{-\frac{\gamma^2(q-q')^2}{40^+}}(q'-q)^2\Big) \\
&= \frac{i}{2}\sqrt{\frac{1}{\pi 0^+}}\int_{-\infty}^{\infty} dq'\,\left[\frac{d}{dq'}\psi(q') - 2\beta q\psi(q')\right]e^{-\frac{\gamma^2(q-q')^2}{40^+}} \qquad (.24)\\
&= \frac{i}{\gamma}\int_{-\infty}^{\infty} dq'\,\delta(q'-q)\left[\psi'(q') - 2\beta q\psi(q')\right] \\
&= \frac{i}{\gamma}\left(\frac{d}{dq} - 2\beta q\right)\psi(q) = \left(-\frac{1}{\gamma}p - \frac{2i\beta}{\gamma}q\right)\psi(q),
\end{aligned}$$

where we have used $p = -i\frac{d}{dq}$ and the properties of the Delta distribution

$$\delta_{0^+}(q'-q) = \frac{\gamma}{2}\sqrt{\frac{1}{\pi 0^+}}e^{-\frac{\gamma^2(q'-q)^2}{40^+}} \quad ,\int_{-\infty}^{\infty} dq'\,\delta(q'-q)\psi(q') = \psi(q).$$

Similarly, the transformed momentum operator is

$$\begin{aligned}
\hat{p}'(q,q') &= \int_{-\infty}^{\infty} dq''\,K^{-1}(q,q'')p''K(q'',q') \\
&= -i\int_{-\infty}^{\infty} dq''\,K^{-1}(q,q'')\frac{d}{dq''}K(q'',q') \\
&= -i\Big(2\alpha\underbrace{\int_{-\infty}^{\infty} dq''\,K^{-1}(q,q'')q''K(q'',q')}_{\hat{q}'(q,q')} + i\gamma q'\underbrace{\int_{-\infty}^{\infty} dq''\,K^{-1}(q,q'')K(q'',q')}_{\delta(q'-q)}\Big),
\end{aligned} \qquad (.25)$$

and its action on a wave function is

$$\begin{aligned}
(\hat{p}'\psi)(q) &= \int_{-\infty}^{\infty} dq'\,\left(-2\alpha i\hat{q}'(q,q') + \gamma q'\delta(q'-q)\right)\psi(q') \\
&= -2\alpha i\left(\frac{i}{\gamma}\left[\frac{d}{dq} - 2\beta q\right]\psi(q)\right) + \gamma\psi(q) \qquad (.26)\\
&= \left(\frac{2\alpha}{\gamma}ip + \left[\gamma - \frac{4\alpha\beta}{\gamma}\right]q\right)\psi(q)
\end{aligned}$$

In summary, the canonical variables transform according to

$$q \to -\frac{1}{\gamma}p - \frac{2i\beta}{\gamma}q \quad ,p \to \frac{2\alpha}{\gamma}ip + \left[\gamma - \frac{4\alpha\beta}{\gamma}\right]q. \qquad (.27)$$

and the canonical commutation relation is preserved

$$\left[q',p'\right] = \left[-\frac{1}{\gamma}p, (\gamma - \frac{4\alpha\beta}{\gamma})q\right] + \left[-\frac{2i\beta}{\gamma}q, \frac{2\alpha}{\gamma}ip\right] = [q,p] = i. \qquad (.28)$$

.2 Additional Figures

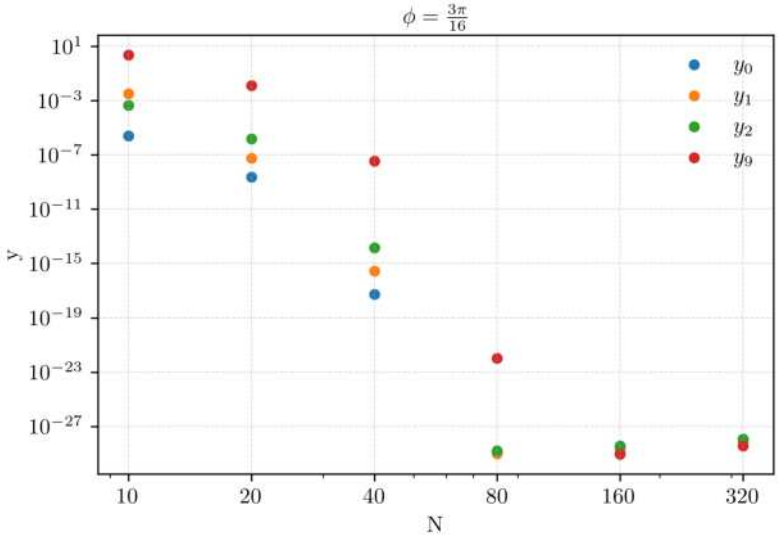

Figure 1: Tail-weight-ratio of the complex deformed harmonic oscillator for $\phi = \frac{3\pi}{16}$. Significant convergence is observed.

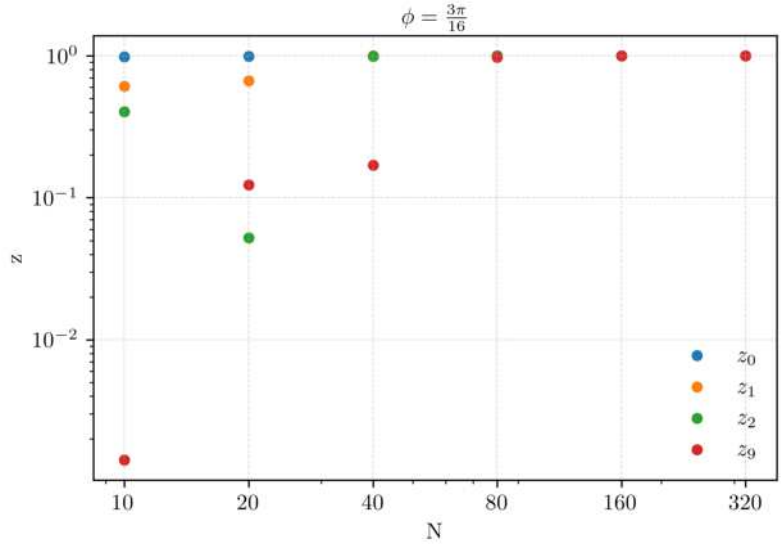

Figure 2: Truncation fidelity of the complex deformed harmonic oscillator for $\phi = \frac{3\pi}{16}$. Significant convergence is observed.

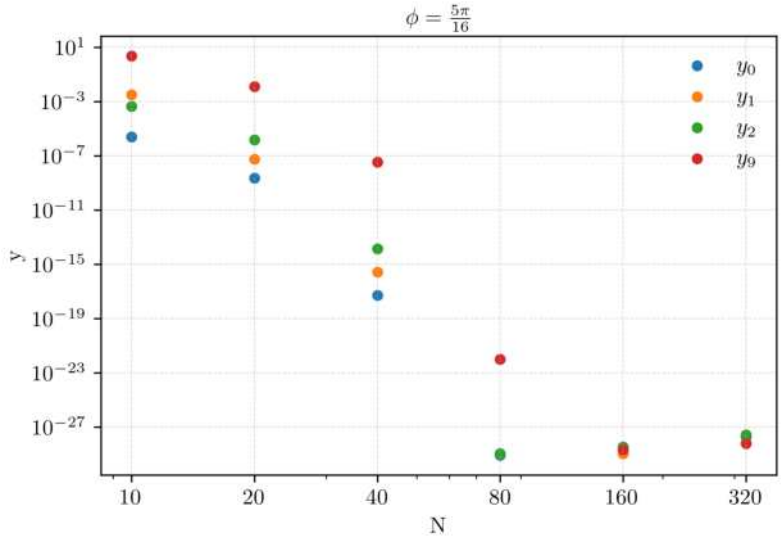

Figure 3: Tail-weight-ratio of the complex deformed harmonic oscillator for $\phi = \frac{5\pi}{16}$. Significant convergence is observed.

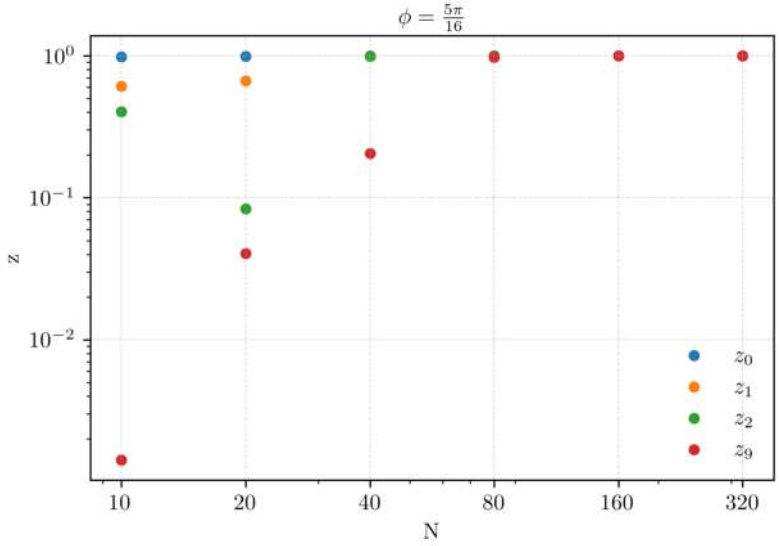

Figure 4: Truncation fidelity of the complex deformed harmonic oscillator for $\phi = \frac{5\pi}{16}$. Significant convergence is observed.

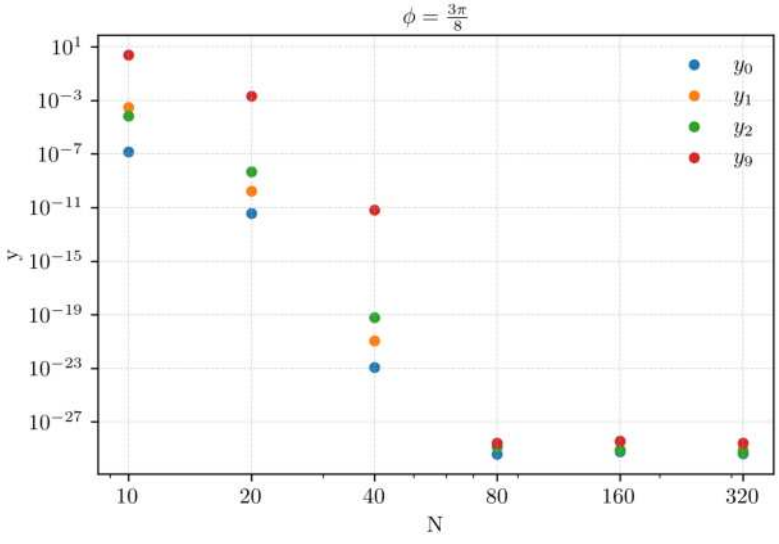

Figure 5: Tail-weight-ratio of the complex deformed harmonic oscillator for $\phi = \frac{3\pi}{8}$. Significant convergence is observed.

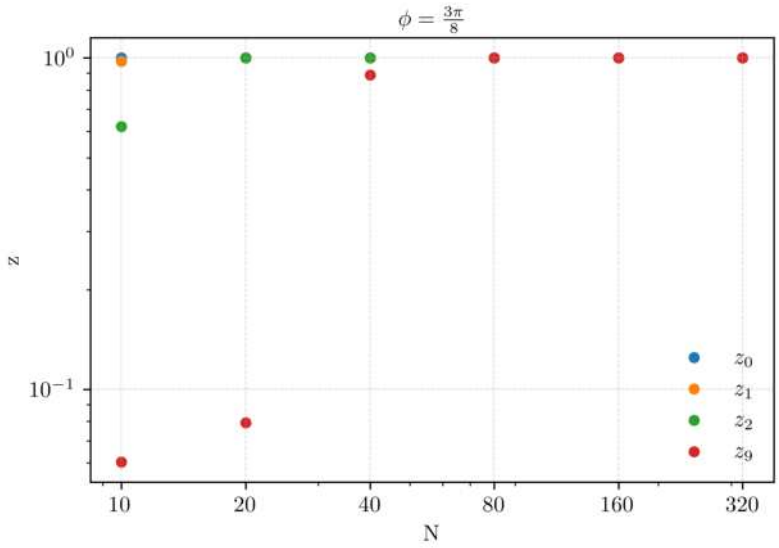

Figure 6: Truncation fidelity of the complex deformed harmonic oscillator for $\phi = \frac{3\pi}{8}$. Significant convergence is observed.

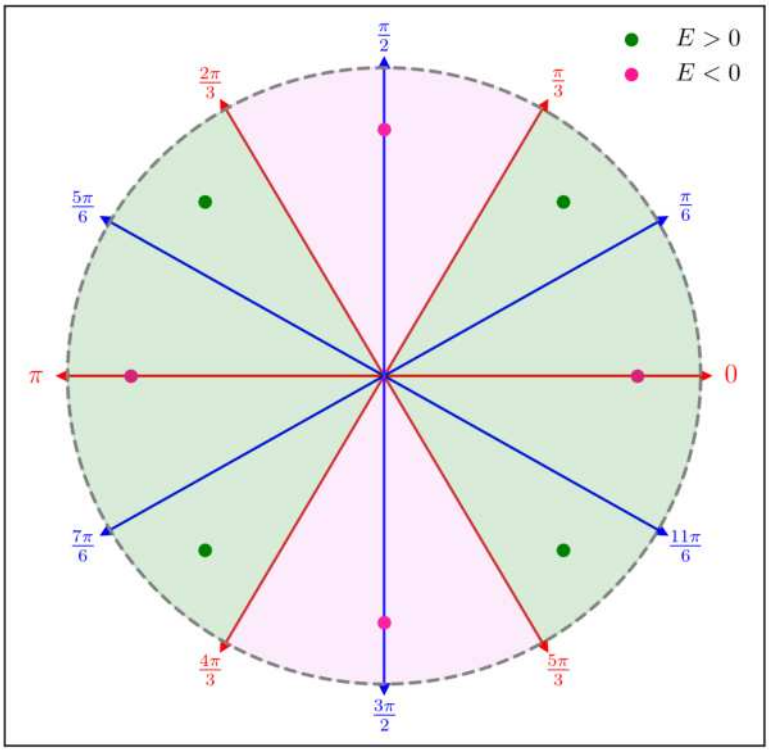

Figure 7: Stokes and anti-Stokes structure of the $-q^4$-potential on the unit circle. The real turnng points with positive energy are marked in green and the turning points with negative energy are marked in pink. In the green sectors, the spectrum takes real eigenvalues with $E > 0$ and in the pink sectors $E < 0$. The real axis is a Stokes line. This is why no spectrum exists here.

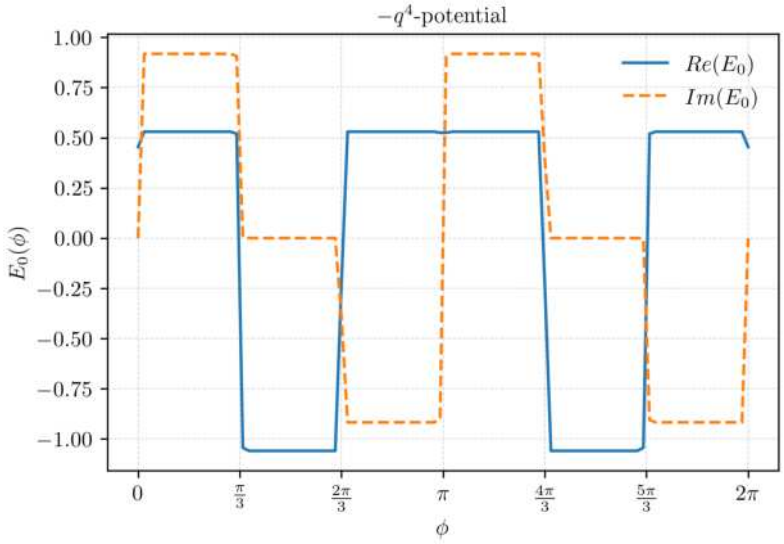

Figure 8: Ground state of the $-q^4$-potential as a function of the angle ϕ.

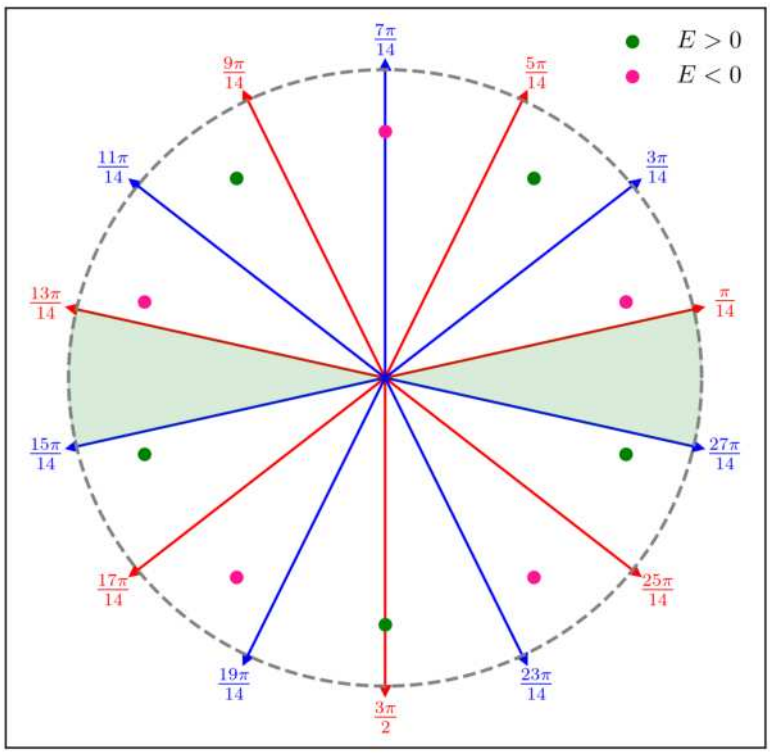

Figure 9: Stokes and anti-Stokes structure of the $-iq^5$-potential on the unit circle. The Turning points with positive energy are marked in green and the turning points with negative energy are marked in pink. In the green sector, the spectrum takes real and positive eigenvalues.

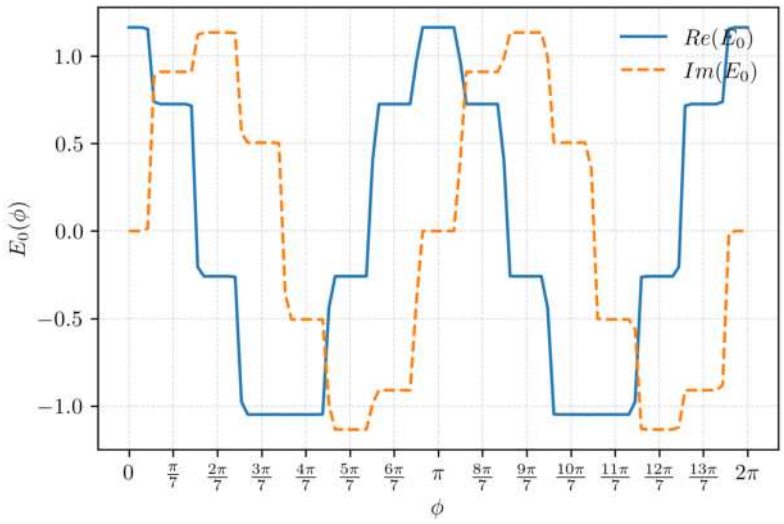

Figure 10: Ground state of the $-iq^5$-potential as a function of the angle ϕ.

Acknowledgments

I am deeply grateful to my supervisor, Steven Kim, and to Prof. Dr. Fabian Hassler for their excellent guidance and support throughout this work, for always providing helpful feedback and for generously sharing their knowledge and experience.
I also appreciate the opportunity to present my progress to the research group; their insightful comments and constructive suggestions were invaluable for the further development of this study.

Bibliography

[1] Fabian Hassler. Quantum mechanics. Lecture notes, RWTH Aachen, 2024.

[2] Ingrid Rotter. Non-hermitian quantum physics of open systems, 2017.

[3] Carl M. Bender and Stefan Boettcher. Real spectra in non-hermitian hamiltonians having $\mathcal{PT}$ symmetry. *Phys. Rev. Lett.*, 80:5243–5246, Jun 1998.

[4] Jan Provazník, Radim Filip, and Petr Marek. Taming numerical errors in simulations of continuous variable non-gaussian state preparation. *Scientific Reports*, 12:16574, 2022.

[5] Catherine Drysdale, Matthew Colbrook, and Michael T. M. Woodley. Computation and verification of spectra for non-hermitian systems. *Phys. Rev. Lett.*, 135:170202, Oct 2025.

[6] Volker Meden. Theoretische physik ii (quantentheorie). Lecture notes, RWTH Aachen, 2025.

[7] Carl M. Bender and Daniel W. Hook. $\mathcal{PT}$-symmetric quantum mechanics. *Rev. Mod. Phys.*, 96:045002, Oct 2024.

[8] George B. Arfken and Hans J. Weber. *Mathematical Methods for Physicists*. Elsevier Academic Press, Amsterdam, 6 edition, 2005.